Calhoun: The NPS Institutional Archive

DSpace Repository

Theses and Dissertations   1. Thesis and Dissertation Collection, all items

1987

Observations of a hydromagnetic wave in the earth's magnetosphere.

Patterson, John Woodward III.; Olsen, Richard C.

http://hdl.handle.net/10945/22836

NAVAL POSTGRADUATE SCHOOL
Monterey , California

THESIS

P24685

OBSERVATIONS OF A HYDROMAGNETIC WAVE
IN THE EARTH'S MAGNETOSPHERE

by

John Woodward Patterson III

December 1987

Thesis Advisor: Richard C. Olsen

Approved for public release; distribution is unlimited

UNCLASSIFIED
TY CLASSIFICATION OF THIS PAGE

REPORT DOCUMENTATION PAGE

PORT SECURITY CLASSIFICATION UNCLASSIFIED	1b RESTRICTIVE MARKINGS
CURITY CLASSIFICATION AUTHORITY	3. DISTRIBUTION / AVAILABILITY OF REPORT Approved for public release; distribution is unlimited
ECLASSIFICATION / DOWNGRADING SCHEDULE	

FORMING ORGANIZATION REPORT NUMBER(S)	5. MONITORING ORGANIZATION REPORT NUMBER(S)

AME OF PERFORMING ORGANIZATION Naval Postgraduate School	6b. OFFICE SYMBOL (If applicable) Code 61	7a. NAME OF MONITORING ORGANIZATION Naval Postgraduate School
DRESS (City, State, and ZIP Code) Monterey, California 93943-5000		7b. ADDRESS (City, State, and ZIP Code) Monterey California 93943-5000

AME OF FUNDING / SPONSORING ORGANIZATION	8b. OFFICE SYMBOL (If applicable)	9. PROCUREMENT INSTRUMENT IDENTIFICATION NUMBER

DRESS (City, State, and ZIP Code)	10. SOURCE OF FUNDING NUMBERS			
	PROGRAM ELEMENT NO.	PROJECT NO.	TASK NO	WORK UNIT ACCESSION NO.

TLE (Include Security Classification)

OBSERVATIONS OF A HYDROMAGNETIC WAVE IN THE EARTH'S MAGNETOSPHERE

RSONAL AUTHOR(S)
Patterson, John W. III

YPE OF REPORT aster's Thesis	13b TIME COVERED FROM _____ TO _____	14 DATE OF REPORT (Year, Month, Day) 1987, December	15 PAGE COUNT 77

PPLEMENTARY NOTATION

COSATI CODES			18. SUBJECT TERMS (Continue on reverse if necessary and identify by block number)
ELD	GROUP	SUB-GROUP	
			Alfven Wave, Hydromagnetic Wave, Pc5, SCATHA

STRACT (Continue on reverse if necessary and identify by block number)

Measurements of a continuous hydromagnetic micropulsation event, which occurred in the pre-dawn magnetosphere on July 29, 1979, are reported as observed by wave and particle instruments onboard the P78-2 (SCATHA) spacecraft. Calculations of the Poynting vector make it clear that the wave is a traveling Alfven wave guided by the earth's magnetic field line. Plasma densities are calculated at $L = 7$. The phase relationship between the plasma flux and the electromagnetic fields is investigated. A self-consistent set of particle density and particle velocity data is determined, in order to verify the measurement of the electric field. Current magnetospheric models predicting Alfven wave speeds, Alfven wave periods and plasma densities are supported by the study.

STRIBUTION / AVAILABILITY OF ABSTRACT UNCLASSIFIED/UNLIMITED ☐ SAME AS RPT. ☐ DTIC USERS	21. ABSTRACT SECURITY CLASSIFICATION UNCLASSIFIED
AME OF RESPONSIBLE INDIVIDUAL . C. Olsen	22b. TELEPHONE (Include Area Code) (408) 646-2109	ᴢᴢc. OFFICE SYMBOL 61-Os

DRM 1473, 84 MAR	83 APR edition may be used until exhausted. All other editions are obsolete	SECURITY CLASSIFICATION OF THIS PAGE

☆ U.S. Government Printing Office: 1986—606-24.

1

UNCLASSIFIED

Observations of a Hydromagnetic Wave
in the Earth's Magnetosphere

by

JOHN WOODWARD PATTERSON III
Lieutenant, United States Navy
B.S., PURDUE UNIVERSITY, 1979

Submitted in partial fulfillment of the
requirements for the degree of

MASTER OF SCIENCE IN PHYSICS

from the

NAVAL POSTGRADUATE SCHOOL
December 1987

ABSTRACT

Measurements of a continuous hydromagnetic micro-pulsation event, which occurred in the pre-dawn magnetosphere on July 29, 1979, are reported as observed by wave and particle instruments onboard the P78-2 (SCATHA) spacecraft. Calculations of the Poynting vector make it clear that the wave is a traveling Alfven wave guided by the earth's magnetic field line. Plasma densities are calculated at L = 7. The phase relationship between the plasma flux and the electromagnetic fields is investigated. A self-consistent set of particle density and particle velocity data is determined, in order to verify the measurement of the electric field. Current magnetospheric models predicting Alfven wave speeds, Alfven wave periods and plasma densities are supported by the study.

TABLE OF CONTENTS

ACKNOWLEDGEMENT

I. INTRODUCTION

A. GEOMAGNETIC MICROPULSATIONS

Geomagnetic micropulsations are low frequency perturbations of the Earth's magnetic field. They are generally short-lived variations whose amplitude is small when compared to the magnitude of the Earth's main field. In contrast to long term variations of the Earth's magnetic field which are of internal origin, geomagnetic micropulsations, as well as magnetic storms, are thought to be generated by solar forces. [Ref. 1]

The gamma, defined as 10^{-9} Tesla, is commonly used when measuring these extremely small magnetic fields. Micropulsations have amplitudes ranging from fractions of gammas to tens of gammas and periods ranging from approximately 0.1 second to 10 minutes. Micropulsations may be divided into two main classes. Those with regular or continuous patterns are called Pc's and those with irregular patterns Pi's. The system used in this paper for categorizing continuous pulsations is described in Table 1. [Ref. 1]

B. CONTINUOUS PC5 OSCILLATIONS

Micropulsations with the longest periods, Pc5's, may have amplitudes near 100 gamma, but generally are seen to have amplitudes of the order of ten to twenty gamma. A

7

group of Pc5's may last from 10 minutes to several hours. Pc5's have been noted to be absent on days of very low magnetic activity and on very disturbed days. They generally occur during the recovery periods of several days which follow moderate magnetic disturbances. [Ref. 1]

TABLE 1
CONTINUOUS PULSATION CLASSIFICATION

Type	Period (sec.)
Pc1	0.2 - 5
Pc2	5 - 10
Pc3	10 - 45
Pc4	45 - 150
Pc5	150 - 600

1. Previous Observations

Magnetic field micropulsations have been observed from ground stations since the 19th Century. In 1861 Stewart observed what he described as a great magnetic disturbance at Kew Observatory [Ref. 2]. Since then thousands of papers have been published concerning micropulsations. Ground station characteristics of Pc5's were summarized by Barfield and McPherron [Ref. 3]. Ground stations report Pc5's most frequently at dawn and dusk. These data indicate that it is common for PC5's to span 60 degrees of longitude. Simultaneous observations by magnetic conjugate ground stations suggested a generation mechanism located near the equator.

With the advent of satellite exploration in the late 1960's the understanding of long period micropulsations was

8

furthered with data taken by satellite magnetometers.
Several studies were made of data taken by spacecraft in
geosynchronous orbit. For example, correlations were
established between micropulsation observations in 1967 from
Applied Technology Satellite 1 (ATS-1) and ground station
data [Refs. 3 and 4]. This analysis showed that the onset
of 85 percent of the events occurred during the expansion
phase of magnetospheric substorms, suggesting that Pc5's
could be generated by storm enhanced ring currents.

In the early 1970's plasma scientists began to
correlate data made available by multiple sensors on
spacecraft. Comparison of magnetic field data and high
energy plasma data, from Explorer 45, with ground station
data showed that Pc5 resonance regions existed in the
magnetosphere at high altitudes [Ref. 5]. It was suggested
that these resonance regions could be perturbed by a drift
mirror instability. A good review of plasma instabilities
is given by Chen [Ref. 6].

ATS-6 provided an early example of combined magnetic
field and plasma flow measurements in 1974 [Ref. 7]. Using
multiple sensors it was possible to calculate the Poynting
vector using measured magnetic fields and inferred electric
fields. This case study showed the existence of a standing
Alfven wave.

Multi-sensor observations have become more common in
the past decade. The addition of mass spectrometers brought

new dimension to magnetospheric research. A recent example is a Pc5 observed by Dynamics Explorer I in July 1982 [Ref. 8]. Using a mass spectrometer, electric field and magnetic field measurements, it was possible to compare simultaneous measurements of the E X B drift velocities and particle derived plasma drift velocities during a Pc5 event. The plasma was shown to be rotating perpendicular to the magnetic field. Complete analysis of the plasma data showed that significant quantities of singly ionized helium, oxygen and nitrogen, as well as hydrogen, were present in the plasma, which was important in matching plasma theory and observations.

GEOS-2 data from the double probe electric field experiment have been reported for Pc5's observed during 1979 [Ref. 9]. Observed correlations between wave amplitude and plasma density data were used to support current hydro-magnetic wave period models.

Multi-satellite observations can be used to address the spatial structure of Pc5's. Combined magnetic field data from the SCATHA, GOES 2, GOES 3 and GEOS 2 satellites were used to examine the structure of a field aligned Pc5 observed in November 1979 [Ref. 10]. The study showed that the wave had an antisymmetric standing structure along the field line, and that the wavelength was much shorter than the field line. These are characteristics that have not yet been explained by existing theories.

Analysis of these observations, leading to the determination of wave modes, growth characteristics and propagation characteristics, enhance the understanding of basic plasma physics and those processes which determine the dynamics and structure of the magnetosphere.

2. Theory

H. Alfven showed, in 1942, that low frequency electromagnetic waves can propagate in fluids of high conductivity in the presence of a constant magnetic field [Ref. 11].

These waves are difficult to observe on a laboratory scale. S. Lunquist determined that for a strong interaction to occur between electromagnetic and hydrodynamic systems the criterion which must be met is

$$BL\sigma(\mu/\rho)^{1/2} >> 1 \qquad (1.1)$$

where B is the magnetic field, L is the dimension of the conducting fluid, σ is the conductivity and ρ is the density of the fluid [Ref. 12]. Since the dimensions of the magnetosphere are large, this type of interaction is possible.

In a Newtonian fluid, of perfect conductivity and density ρ, small perturbations of the magnetic field, B_o, will propagate along the magnetic field line with velocity given by

$$V_A = \omega/k = B_o / (\mu_o\rho)^{1/2} \qquad (1.2)$$

which is called the Alfven velocity [Ref. 6].

In 1952, Alfven compared hydromagnetic waves to the vibrations of an elastic string with its ends fixed at magnetic field conjugate points [Ref. 13]. A good summary of the analogy is given by Sugiura and Wilson [Ref. 14]. The derivation of this analogy is described showing that the plasma acts as the mass of the string. The calculation of perturbation modes of these string vibrations, as applied to the earth's magnetic field, is presented.

Hasegawa and Chen separate the theory of long period micropulsations into two categories and set forth a theory for each type [Ref. 15]. One type can be explained as a resonant Alfven wave excited at a local field line by a Kelvin-Helmholtz instability at the magnetopause. The second type is interpreted as an excitation of a surface eigenmode, a Kinetic Alfven Wave, excited by an impulse energized ring current.

In this paper a Pc5 event is described which exhibits some characteristics of a classical Alfven wave. Its source is believed to be the ring current which generates a traveling wave along the magnetic field line.

C. COORDINATE SYSTEMS

The coordinate systems pertinent to this analysis of the Pc5 data are shown in Figure 1. The magnetic field components (B_x, B_y, B_z) are described in topographic coordinates. X is defined as North, Y points East, and Z points down,
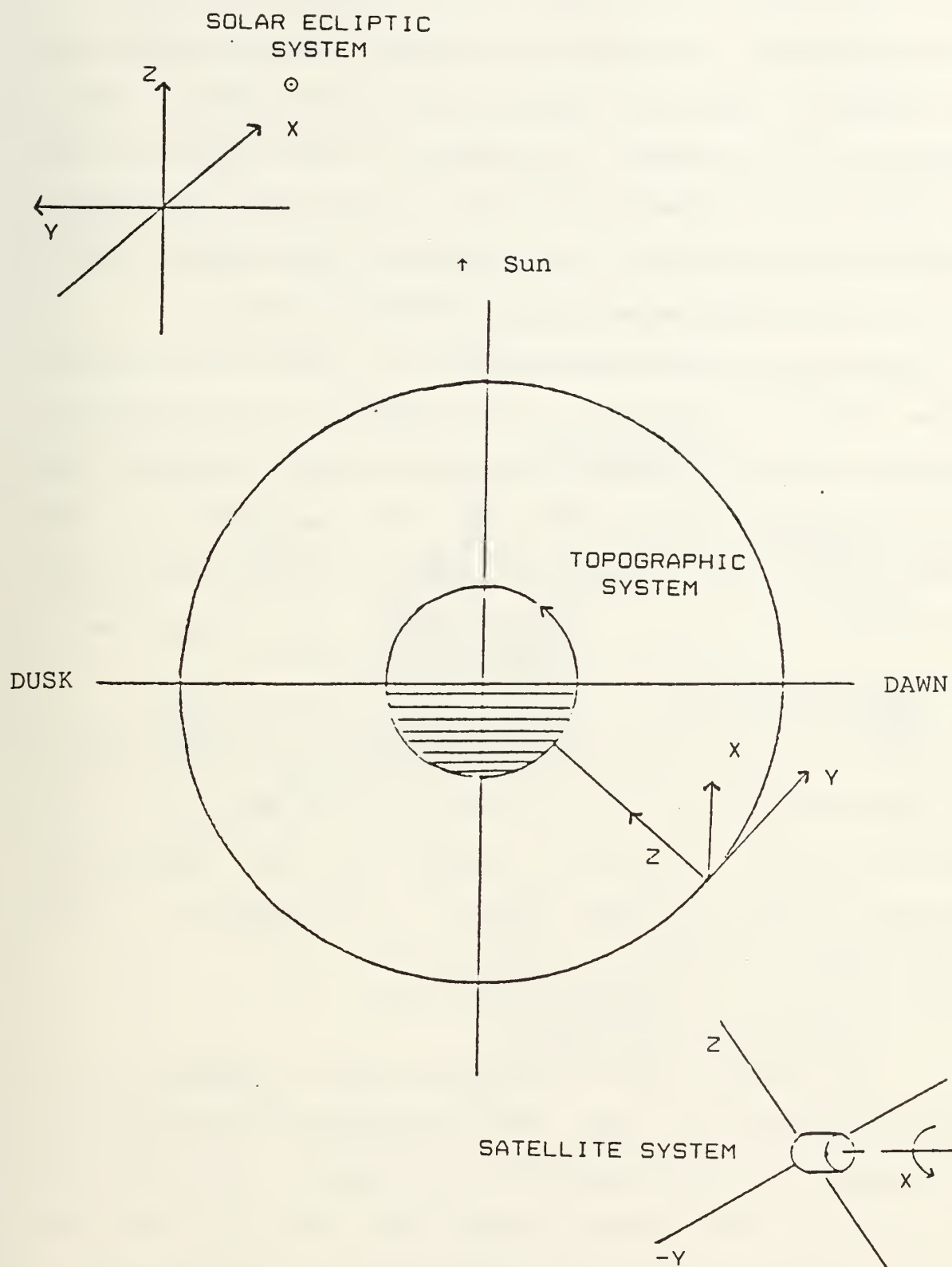
Figure 1.   Coordinate Systems

toward the center of the earth, in the radial direction.

The electric field data are despun into two components (E_X and E_Z) of the solar ecliptic coordinate system. The X direction in this system is parallel to the earth-sun line and points in the sunward direction. The Y axis is perpendicular to the earth-sun line and points toward dusk. The Z axis is right-hand perpendicular to the X-Y plane.

The satellite coordinate system is a rotating coordinate system with X pointing in the direction of the satellite spin axis, which is essentially held constant throughout the orbit. The spin axis is nearly anti-parallel to Y (SE). The Y and Z axis rotate through the plane perpendicular to the spin axis.

D. SCATHA SATELLITE

The U. S. Air Force P78-2 satellite was launched into a near-geosynchronous orbit in January 1979 as part of a joint NASA/Department of Defense program to study Spacecraft Charging At High Altitudes (SCATHA). A schematic of the SCATHA vehicle is shown in Figure 2.

1. SCATHA Orbit Parameters

The SCATHA orbit is elliptical with a perigee of 5.5 Re and an apogee of 7.7 Re. The inclination of the orbit is 7.5 degrees and the period is 23.5 hours. The satellite spin period is 59.5 seconds, with a spin axis in the orbit plane and perpendicular to the earth-sun line. [Refs. 16 and 17]

14

UCSD PLASMA DETECTOR

FORWARD END

GSFC ELECTRIC FIELD EXP.

GSFC MAGNETOMETER
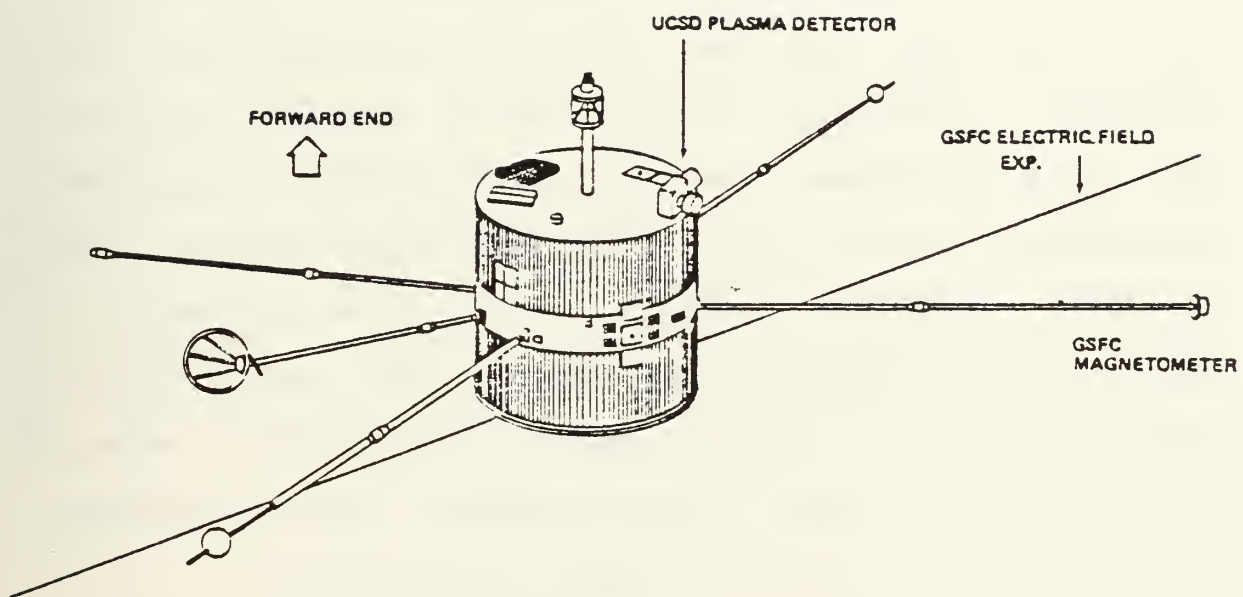
SCATHA SPACE VEHICLE (P78-2)

Figure 2.   Schematic of the SCATHA Satellite

15

Figure 3 shows the satellite's radial distance from the earth's center in earth radii, (1 Re = 6378 km), for the 24 hours of Day 210. The Pc5 is observed from 4 to 7 hours UT during a continuous decline in SCATHA's radial distance. Figures 4 and 5 show the geographic latitude and longitude during the same period. During the Pc5 event the geographic latitude and longitude remain nearly constant. The variation in SCATHA's latitude is a result of the 7.5° inclination in the orbit. The variation in longitude reflects the fact that the orbit is not geosynchronous, but elliptical. The result of the slighly inclined elliptical orbit is a continuous change in the satellite's geographic longitude as well as it's velocity and radial distance from the earth. SCATHA's velocity varies from 2.55 km/s, at apogee, to 3.74 km/s, at perigee. The virtue of this slightly elliptical orbit is that the satellite can sweep a wide sector of the earth's magnetosphere while introducing only small errors in the raw magnetospheric data.

In the analysis of magnetospheric data, the satellite's location relative to the earth's magnetic field is important in the classification of observed phenomena. A first approximation of the shape of the earth's magnetic field is that of a dipole given by

$$R = r \sin^2\theta \qquad (1.3)$$

where r is the distance from the earth's center to the
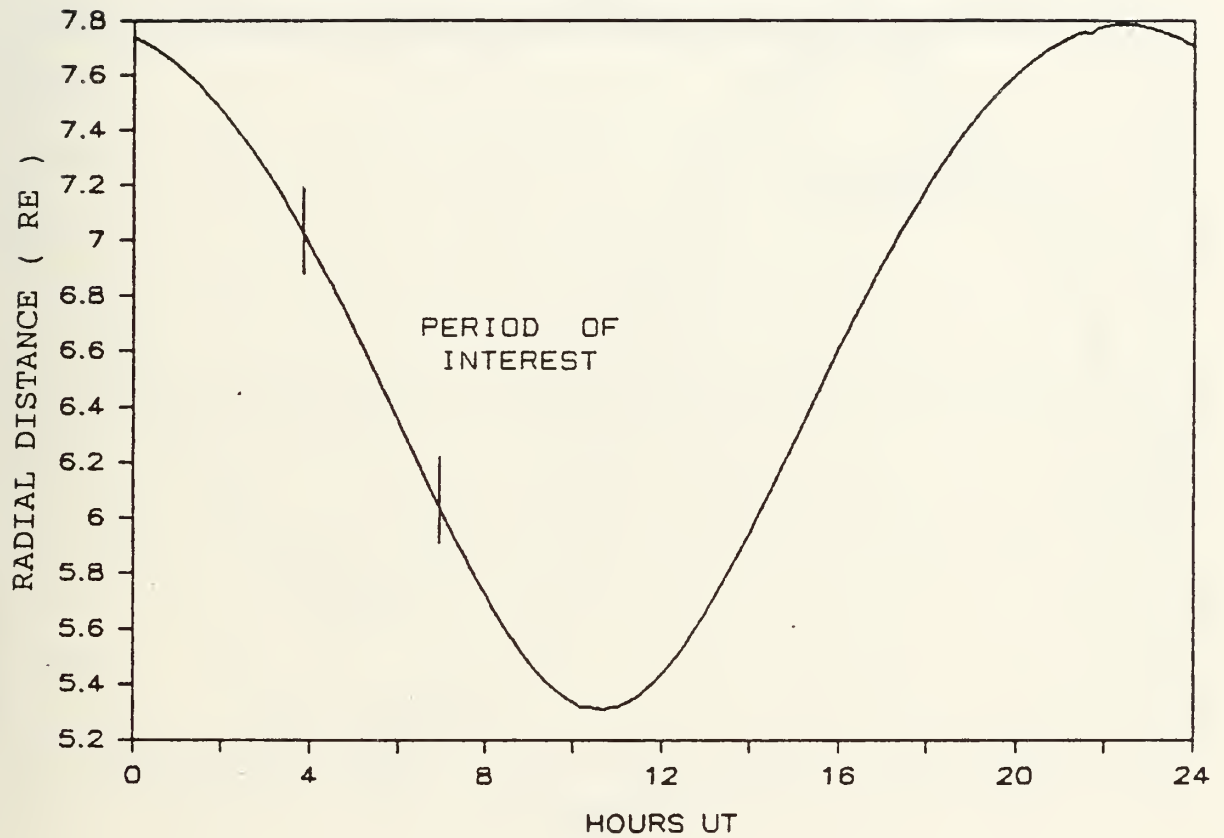
SCATHA DAY 210

Figure 3. Radial Location of SCATHA on July 29, 1979

17
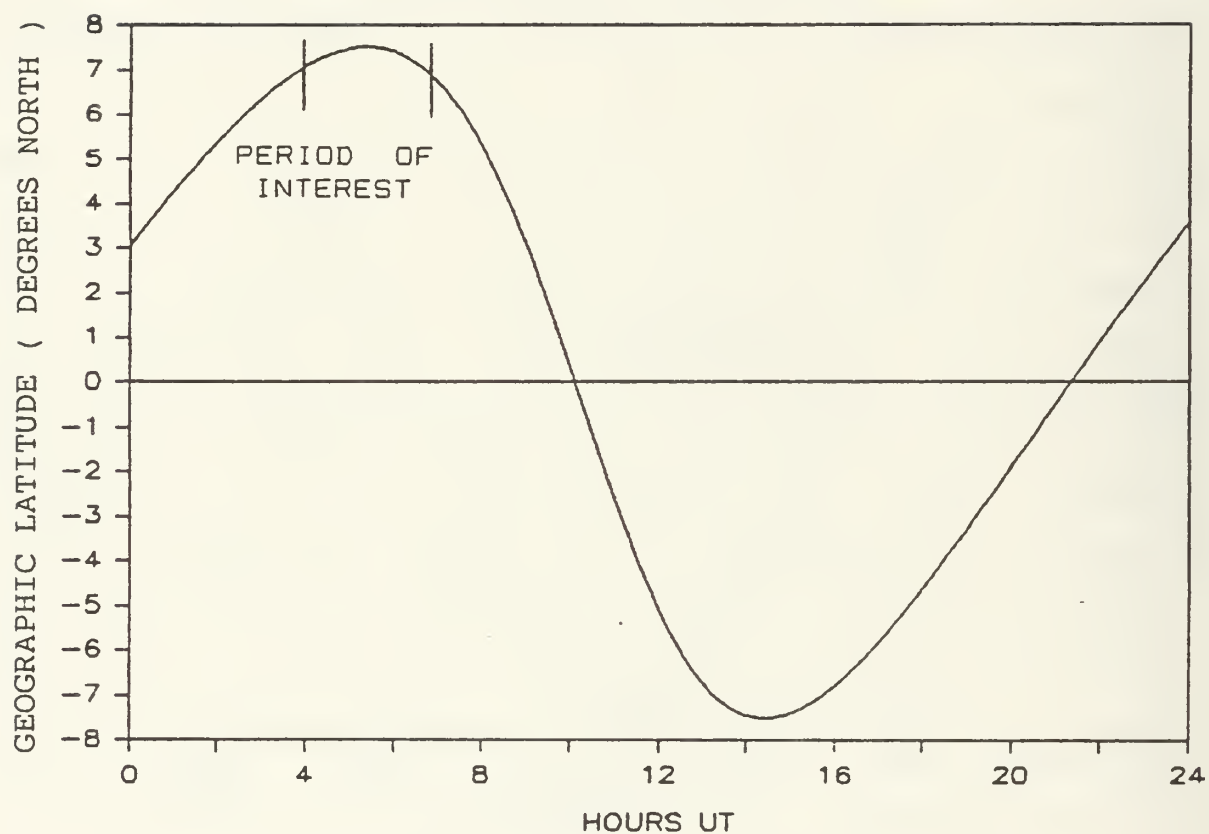
Figure 4.   Geographic Latitude of SCATHA on July 29, 1979

18
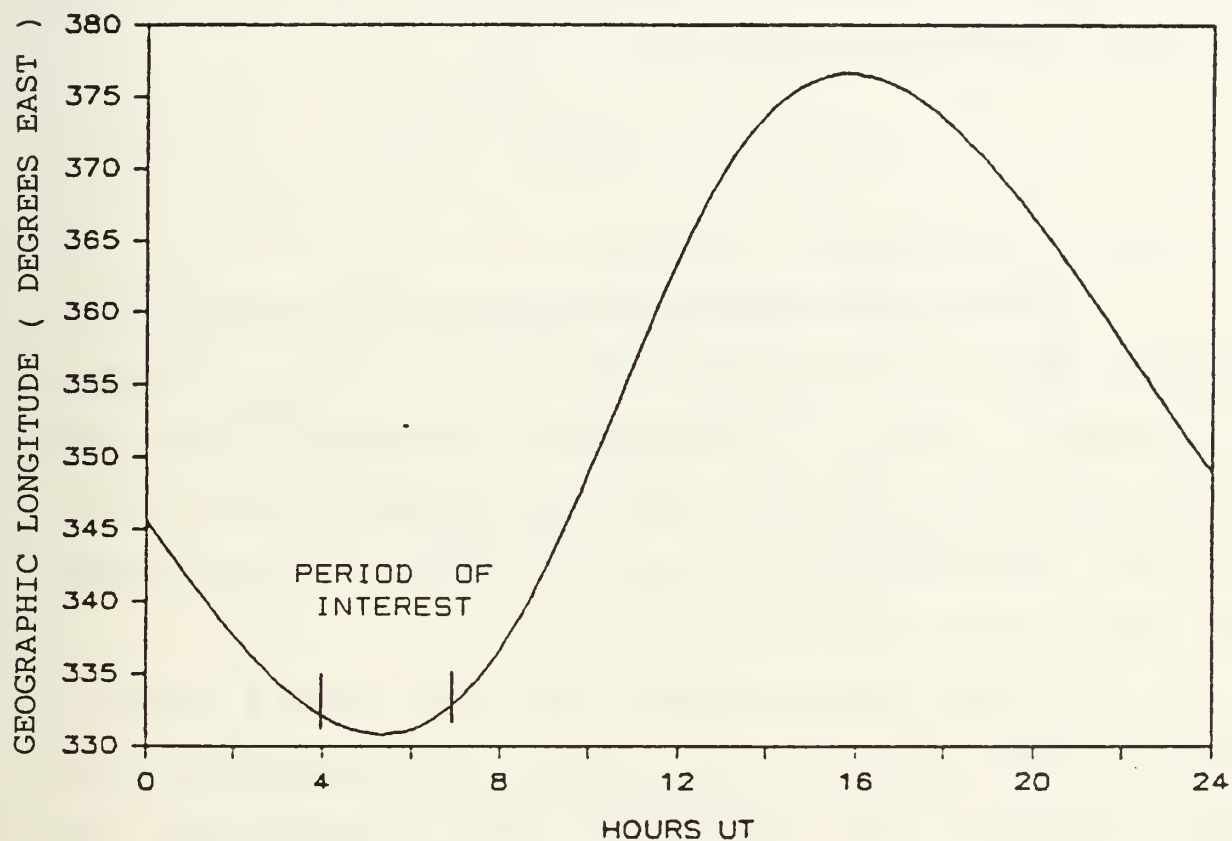
SCATHA LONGITUDE

Figure 5.   Geographic Longitude of SCATHA on July 29, 1979

19

intersection of the dipole field line with the equatorial
plane. R and θ are the polar coordinates of the magnetic
field line. The parameter used to define the location of a
magnetic field line is the McIlwain L [Ref. 18]. Using the
dipole approximation for the magnetic field, the L of the
field line is equal to the number of earth radii at which
the field line crosses the equatorial plane. The value of L
at other latitudes is given by

$$L = Re / \cos^2\theta_m \qquad\qquad (1.4)$$

where θ_m is the magnetic latitude.

A view of the magnetic field dipole approximation is
shown in Figure 6 where field lines for L = 5, 6, 7, and 8
are plotted. Scatha's dipole magnetic position between 0400
UT and 0700 UT is plotted. At 0400 UT SCATHA was at L =
8.03 and descended to L = 6.59 at 0700 UT. It is during
this period that the Pc5 was observed.

The dipole approximation for the earth's magnetic
field is most exact at dawn and dusk. The approximation is
fairly inexact at noon (where the field is compressed) and
poor at midnight (where the field is extremely elongated).
The distortion of the earth's magnetic field is largely due
to the solar wind. A more exact description of the shape of
the magnetic field is given by Hess [Ref. 19].

20
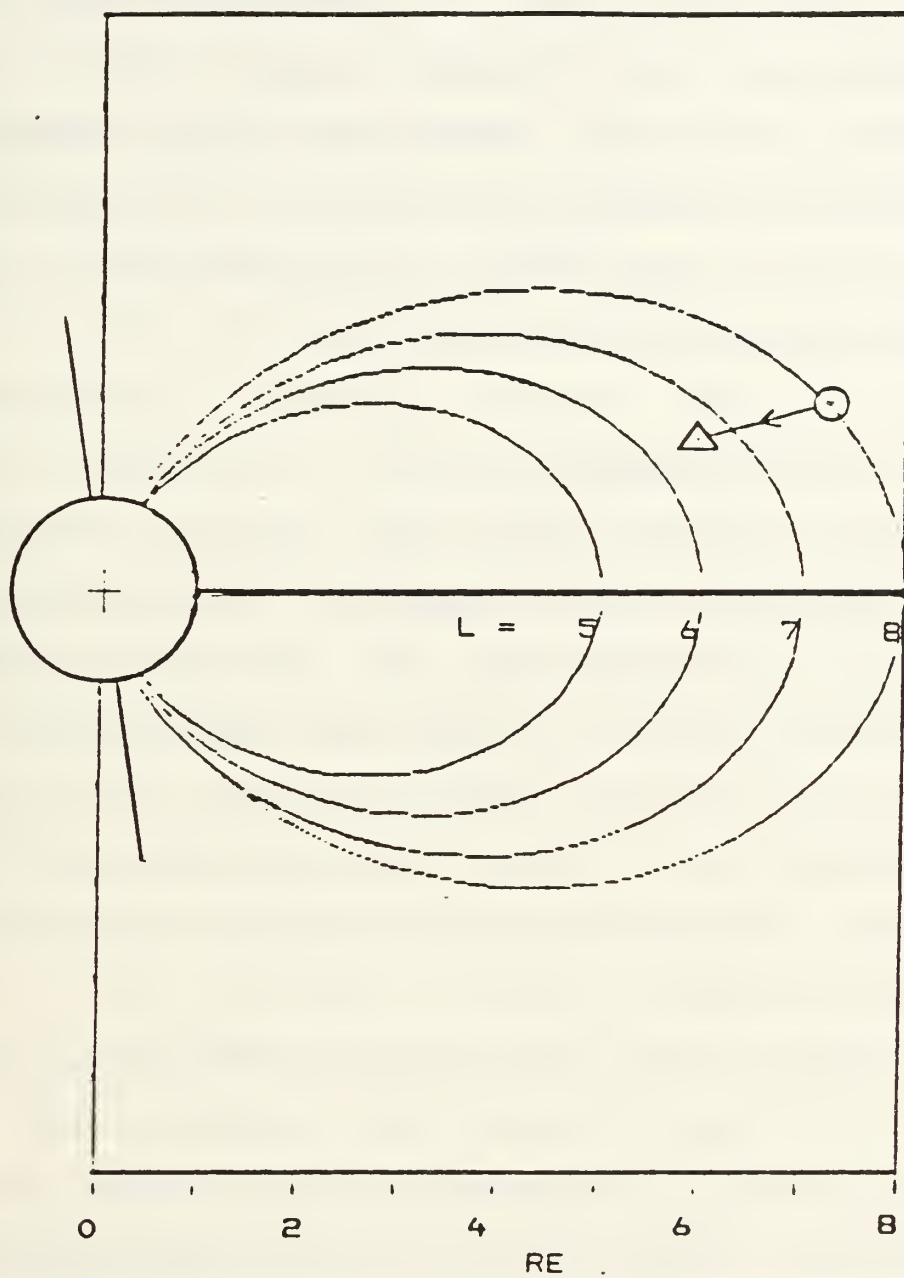
△   SCATHA POSITION AT 0700 UT

O   SCATHA POSITION AT 0400 UT

Figure 6.   McIlwain L and Geomagnetic Latitude of the Pc5

2. Instruments

The spacecraft is a cylinder approximately 1.75 meters in length and diameter. The instruments used in this study are the NASA Goddard Space Flight Center electric field monitor, the NASA Goddard Space Flight Center magnetometer and the University of California, San Diego (UCSD) charged particle experiment. The locations of these instruments are shown in Figure 2. [Ref. 17]

a. The NASA Goddard electric field detector consists of two antennas that are 50 meters in length projecting into the spin plane which are used as floating probes. The antenna wire is composed of beryllium copper. Each antenna is insulated except for the last 20 meters, which is the active part. Differential signals between the antennas give the ambient electric fields. The minimum measurable field is 0.05 mV/m. The time resolution of the electric field measurements is limited by the satellite spin period (59.5 seconds).

SCATHA data are despun into the X and Z components of the solar ecliptic (SE) coordinate system. By this method the two components of the measured electric field (E_X and E_Z), which are in the plane perpendicular to the satellite spin axis are known. It will be shown that the E_Z component of the field data reflects the component of the Pc5 electric field which is perpendicular to the earth's magnetic field when the satellite is near local dawn. The

22

transformation from the measured fields to the ambient fields requires the addition of a 0.3 mV/m sunward field to account for satellite motion. [Refs. 16 and 17]

b. The GSFC magnetometer is a triaxial flux gate magnetometer mounted on a 4 meter boom. The resolution is 0.3 gamma with four vector measurements per second. Data from the GSFC magnetometer are used in raw form and despun into the three vectors listed of the topographic coordinate system. [Refs. 16 and 17]

c. The UCSD charged particle experiment is an electrostatic analyzer that measures both ion and electron flux. Particle data from the electrostatic analyzers (ESAs) are used to measure the ion and electron distribution functions and deduce the particle density, temperature and velocity. The UCSD particle detectors consist of five ESAs arranged in two rotating pairs of electron and ion detectors, and one fixed ion detector. All three of the sensors of this instrument are contained in a single package mounted on the forward end of the satellite. [Refs. 16 and 17]

One of the pairs of rotating detectors covers the energy range from 1 eV to 81 keV (the N/S detectors). The other pair (the E/W detectors) and the fixed detector cover the 1 eV to 1800 eV energy range. The analyzers have energy resolution of 20% ($\delta E/E$) and require 16 seconds for one 64 step energy scan. [Refs. 16 and 17] A more complete

description of the satellite and instrumentation is contained in the IMS Source Book [Ref. 20] and the P78-2 Technical Report [Ref. 21].

II. OBSERVATIONS

A. PARTICLE AND FIELD DATA

During the morning hours of Day 210 SCATHA recorded a disturbance in the earth's magnetic field, beginning at L = 7.96, as the spacecraft approached the maximum inclination of its orbit, 7.5 degrees. A strong magnetic field micropulsation, a Pc5, was recorded on each of SCATHA's sensors.

Figure 7 is an equatorial plane plot of SCATHA's orbit on July 29, 1979 (Day 210). The location of the extremes of the SCATHA orbit are shown with respect to the earth sun line. The sector of the orbit, in which the Pc5 event was observed, is also indicated in Figure 7.

1. Magnetic Field Data

Figure 8 shows the SCATHA magnetic field data recorded from 0300 UT to 0800 UT. Included are the total magnetic field, B_O, and the three topographic components of the field (B_x, B_y, B_z). The significant rise in the magnitude of B_O, the total field, and B_x, the northerly component, is due to the continuous descent of the spacecraft through the earth's magnetic field for that period of it's orbit. During that time period, SCATHA's radial distance diminishes from 7.3 Re to 5.3 Re, and L decreases from 8.28 to 6.16.

SCATHA DAY 210 ORBIT
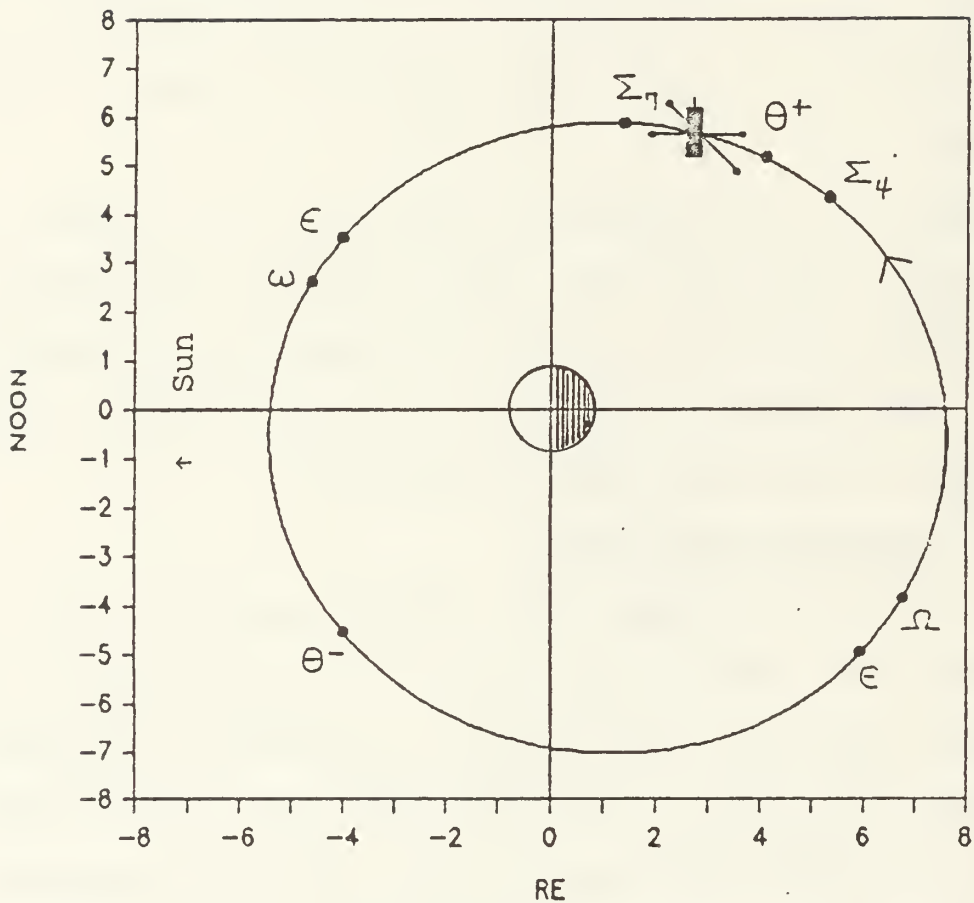
Σ4 ≡ FIRST OBSERVATION OF THE PC5
θ+ ≡ MAXIMUM INCLINATION OF THE ORBIT
Σ7 ≡ LAST OBSERVATION OF THE PC5
ε ≡ ORBIT CROSSES EQUATOR
ω ≡ PERIGEE
θ- ≡ MINIMUM INCLINATION OF THE ORBIT
Ω ≡ APOGEE

Figure 7.   Equatorial Plane Plot of SCATHA Orbit

26
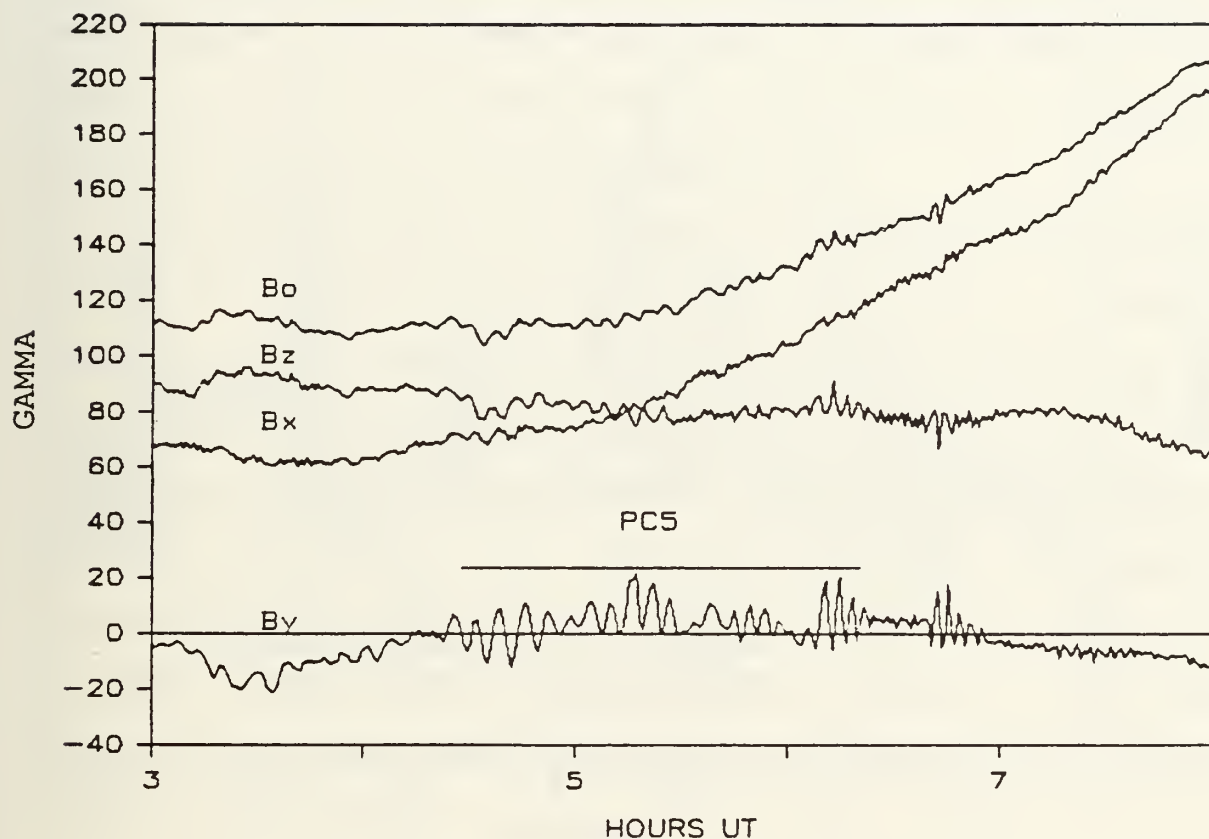
Figure 8.   Magnetic Field Data from 0300 to 0800 UT

27

EAST-WEST MAGNETIC FIELD (By)
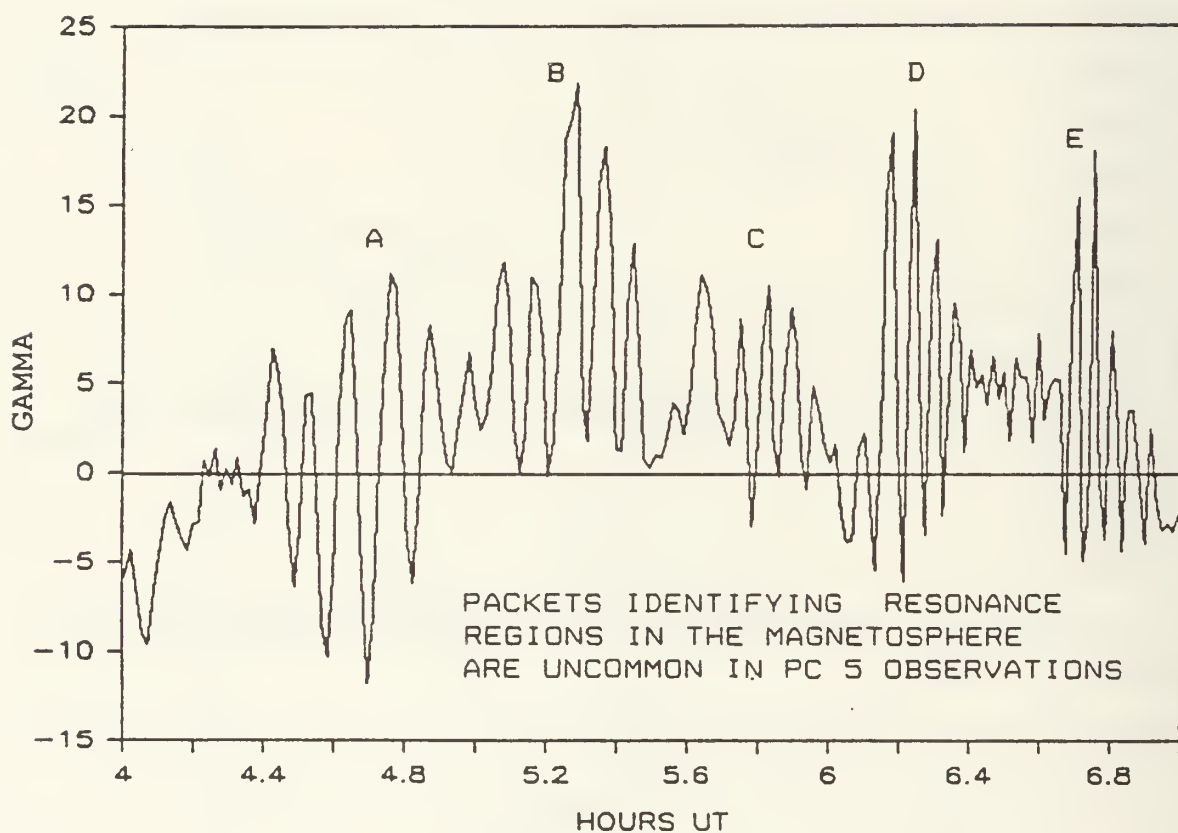
Figure 9.   The Pc5 in the East-West Component
of the Magnetic Field

The amplitude of the radial component of the magnetic field, B_z, varies from 1 to 4 gamma during this period. The magnitude of this component is largely due to the tilt of the earth's main magnetic field vector in the Z direction. The perturbations in B_z are a result of a small component of the Pc5 in that direction. The Pc5 is observed in the plot of the east-west component of the field, B_y, beginning at 4:16 UT and continuing until just before dawn, 06:56 UT. Since the perturbations in B_x and B_z are small, the Pc5 event is largely contained in B_y.

The B_y data are expanded in Figure 9 for the time period 0400 to 0700 UT (2:14 to 5:21 local time). A characteristic of this Pc5, which makes it fairly unique, is the packetized nature of the pulsations. These packets imply different regions of hydromagnetic resonance in the magnetosphere. The packets are labelled A through E for convenience in comparison to the electric field data which follows. The period of the pulsations decreases with time. It will be shown that the period is a function of L and of the particle density.

2. Electric Field Data

Figure 10 is a plot of the electric field data measured by SCATHA from 0300 to 0800 UT. As mentioned earlier, the electric field data is despun into two components of the solar ecliptic (SE) coordinate system. The E_x component points in the sunward direction and remains

DAY 210 ELECTRIC FIELDS
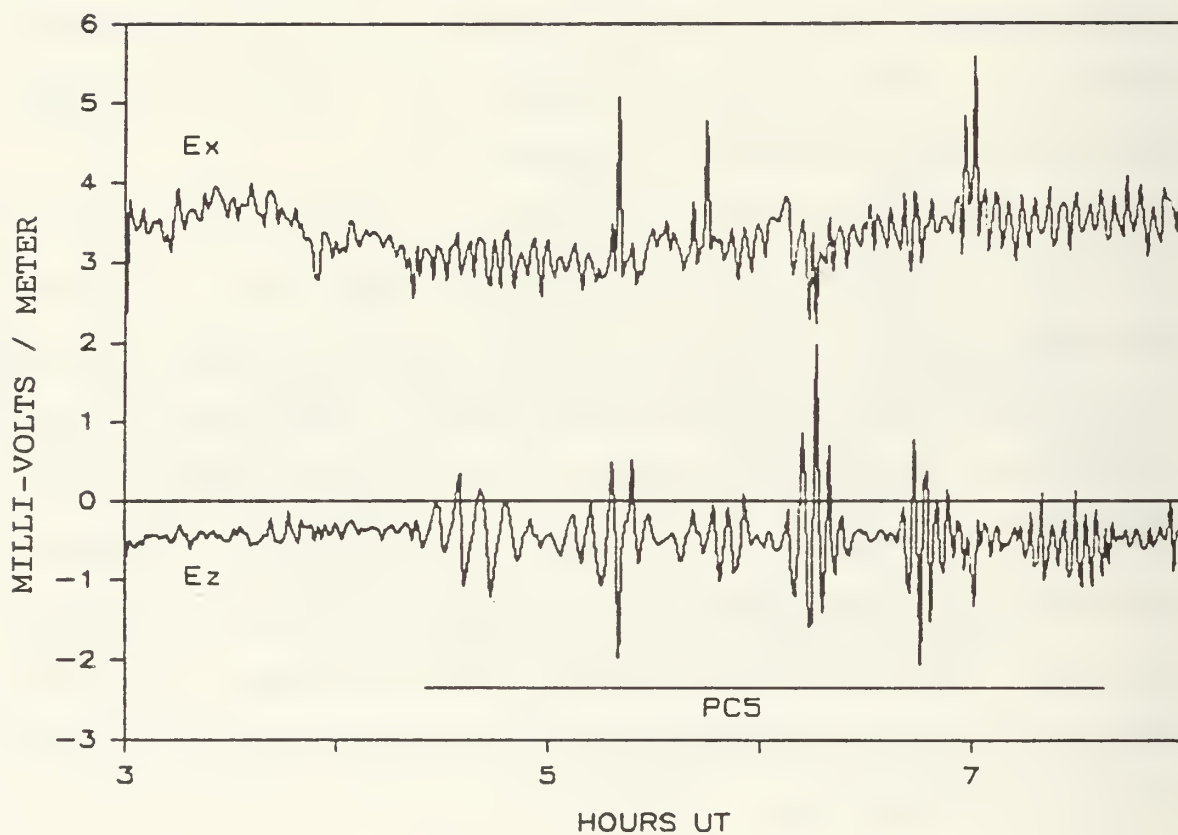
Figure 10.   Electric Field Data from 0300 to 0800 UT

30

almost constant at 1.5 mV/m throughout the event (2 mV/m has been added to the value of E_x, in Figure 10, in order to separate E_x from E_z). This component is a result of the SCATHA's relative motion through the plasma, the static convective electric field, the sunward electric field caused by photoemission [Ref. 17] and a partial projection of the Pc5 electric field perturbation vector in the X direction.

The E_z component is perpendicular to the solar ecliptic plane. This component is nearly equal to the total electric field component of the Pc5. A -0.43 mV/m offset seen in the data is attributed to error fields and a steady state convective field.

Figure 11a is an expanded plot of E_z from 0400 UT to 0700 UT. The packetized nature seen in the magnetic field pulsation is reflected in the electric field. For convenience, the electric field data is seperated into named resonance packets as listed in Table 2.

TABLE 2
HYDROMAGNETIC RESONANCE PACKETS

Packet	t begin	t end
	(hours UT)	
A	4.41	4.90
B	5.03	5.46
C	5.65	6.02
D	6.10	6.40
E	6.63	6.95

The component of the electric field, E_p, which results from a perturbation in B_y (topographic coordinates).

ELECTRIC FIELD (Ez)
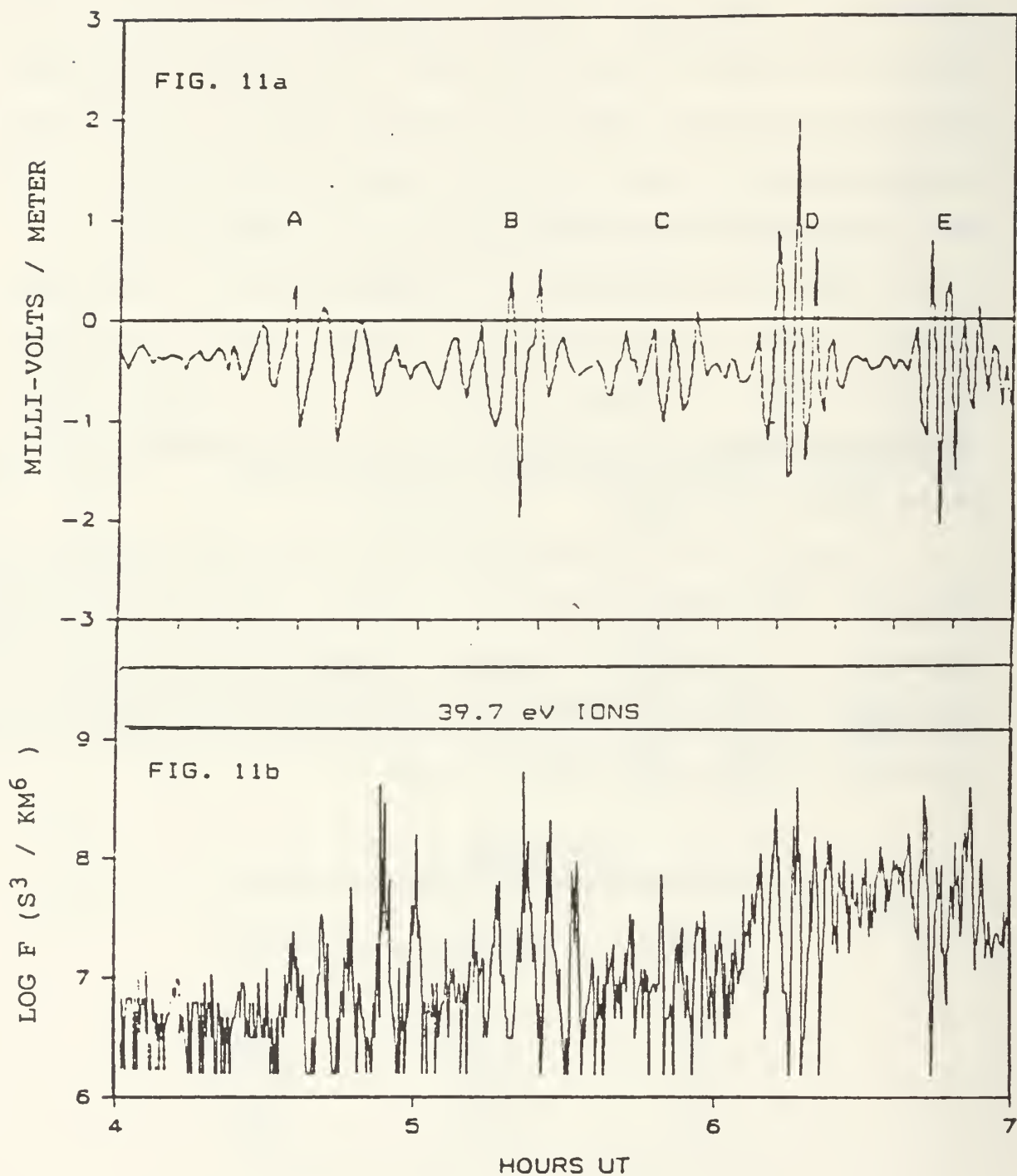
Figure 11. Measured Electric Field and Low Energy Ion
Distribution Function Showing Modulation
of Ion Flux by the Field

32

should be perpendicular to both B_y and B_o. E_z (SE coordinates) is believed to be a projection of E_p onto the electric field antenna. This is based on the assumption that there can be no component of the electric field sustained in the direction of B_o.

$$\delta \vec{E} \cdot \vec{B_o} = 0 \qquad (2.1)$$

The electrons in a plasma are free to move along the magnetic field line and quickly reduce any potential difference which might be impressed along that direction.

Figure 12 shows the geometry for extracting E_p from E_z. Here α is the angle between B_x and B_o and also the angle between the radial direction and E_p. β is the sum of the satellite's geographic latitude and the satellite's inclination from the solar ecliptic plane. The angle Φ between E_z and E_p is given by

$$\Phi = 90 - (\alpha + \beta) \qquad (2.2)$$

$$E_p \sim E_z / \cos \Phi \qquad (2.3)$$

Table 3 lists these angles and the correction factors, ε, for calculating E_p for the hours of 0400 to 0700 UT. The worst case value is only 60 percent. The correction factor in Table 3, ε, is used as follows:

$$\varepsilon = 1 / \cos \Phi$$

$$|E_p| \sim |E_z| \cdot \varepsilon \qquad (2.4)$$

33
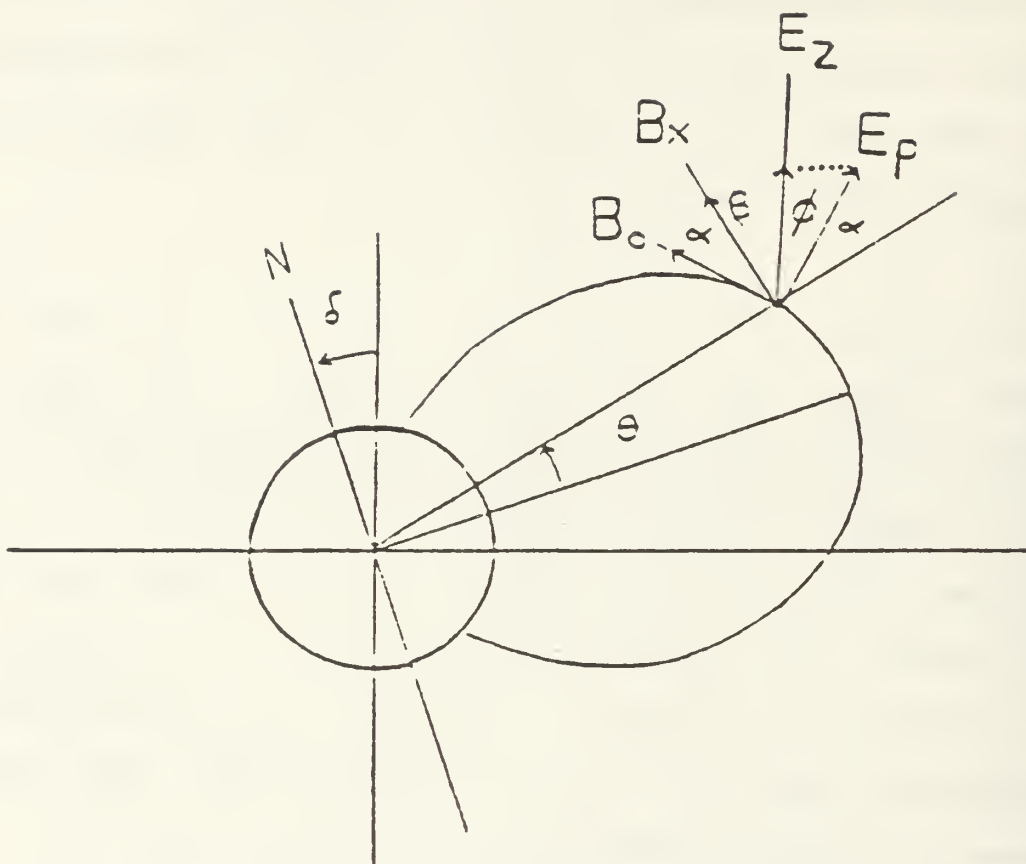
$\alpha \equiv$ ANGLE BETWEEN MAGNETIC FIELD LINE AND B_x

$\delta \equiv$ INCLINATION OF EARTH AXIS ON DAY 210 (18.4°)

$\Theta \equiv$ GEOGRAPHIC LATITUDE OF SCATHA SPACECRAFT

$\beta \equiv$ INCLINATION OF SATELLITE FROM SOLAR ECLIPTIC PLANE.

$$\beta = (\Theta + \delta) \text{ AT LOCAL MIDNIGHT}$$
$$\beta = \Theta \qquad \text{ AT LOCAL DAWN}$$

$$\Phi = 90 - (\alpha + \beta)$$

$$E_P = E_Z/\cos \Phi$$

Figure 12. Calculation of E_p

34

TABLE 3
ELECTRIC FIELD DATA CORRECTION FACTORS

t (UT)	α	β	Φ	ε
		(degrees)		
0400	54.4	19.2	16.4	1.04
0430	50.1	18.0	21.9	1.08
0500	47.8	16.7	25.5	1.11
0530	41.3	15.2	33.5	1.20
0600	37.6	13.4	39.0	1.29
0630	32.9	11.5	45.6	1.43
0700	28.7	9.2	52.1	1.63

The factor which most affects the magnitude of this correction is the shape of the earth's magnetic field at different locations in the orbit. It can be seen in Figure 12 that, for small α, less of the perpendicular field is projected onto the E_z antenna. Near midnight the field is extremely elongated giving a large angle between B_o and B_x, and thus a small angle between E and the Z antenna. At dawn the magnetic field most closely approaches a dipole and so this angle is small. During the analysis of the electric field, with this small correction in mind, the actual electric field data will be assumed to represent the perpendicular electric field ($E_z \sim E_p$).

3. Low Energy Ions

Figure 11b shows a plot of the log (base 10) of the distribution function of the 39.7 ev ions measured from 4 to 7 hours UT. The Pc5 can be seen in the ion flux. A comparison of this plot with the electric field shows that the 39.7 ev ion flux is modulated in phase with the

perturbation of the electric field, δE_z. This reflects the convective drift induced in the ions by the electric field. Higher energy ions and electrons are also modulated, as shown in the expanded presentation of the D packet which follows.

B. A CLOSER LOOK, THE D PACKET

Since the D resonance packet exhibits the largest amplitude fields, it was chosen for closer analysis. This packet begins at 6.1 hours UT and ends at 6.4 hours UT. At this time SCATHA is at 7.3° North, having recently passed the maximum inclination of the orbit. The D packet is observed for a period of 17.23 minutes. The center of this region is at L = 6.97 and at 4:21 local time. During this time SCATHA's average velocity was 3.25 km/sec. After taking into account the decrease in SCATHA's radial position through this period, this resonance packet appears to span an arc of 3300 kilometers.

1. Field Relationships

Figure 13 shows plots of spline fitted E_z and B_y versus time for the D packet. Within the resonance region, E leads B by an average of 130° ± 10°, ($\sim 3\pi/4$), and the average period of the pulsations is 224 seconds. Averages are used since the periods and phases are continuously changing, as if the fields are driven by a multi-frequency or non-harmonic force. The electric field amplitude varies from 0.62 to 1.8 mV/m. The magnetic field amplitude varies

36
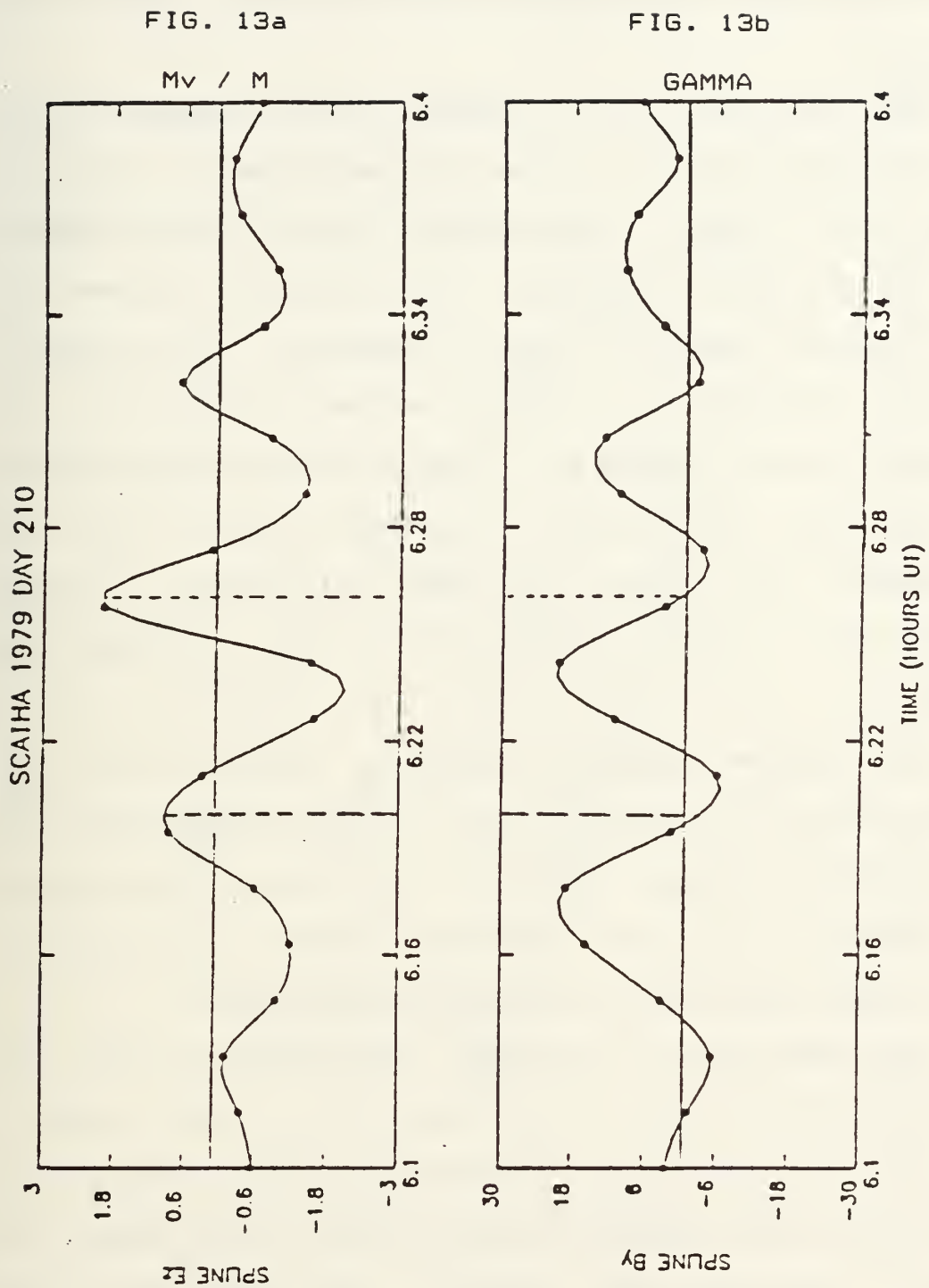
Figure 13.   Pc5 Electric and Magnetic Fields
(D Packet)

37

from 6 gamma to 12 gamma. The large amplitudes at the center of the packet distinguish the center of resonance in this region.

The electric field vector and the magnetic field vector of the Pc5 lie in a plane perpendicular to the main magnetic field line. The electric field vector pulsates toward and away from the earth in a direction between the radial direction and the (SE) +Z direction. The magnetic field vector pulsates in a nearly east-west direction. If the fields were in phase the wave would be propagating in the -X direction (south along the magnetic field line). A standing wave will exhibit $\pi/2$ phase difference. A phase difference of $-\pi$ would indicate the wave is propagating northward.

The average phase of fields in Figure 13 is $3\pi/4$. This implies that the wave is not a pure propagating wave. The continuously changing phase of the fields and the motion of the spacecraft through different regions of resonance make the phase interpretation somewhat ambiguous.

The complexity of the phase relationship is born out by a phase hodogram plot of δE_z versus δB_y in the D packet, Figure 14. In a hodogram a propagating wave would give a diagonal line, and a standing wave a circle (if E and B are plotted in Volts/meter and Tesla). This hodogram implies that the wave is propagating at times, where the plot is nearly linear. At other times it shows the phase of a
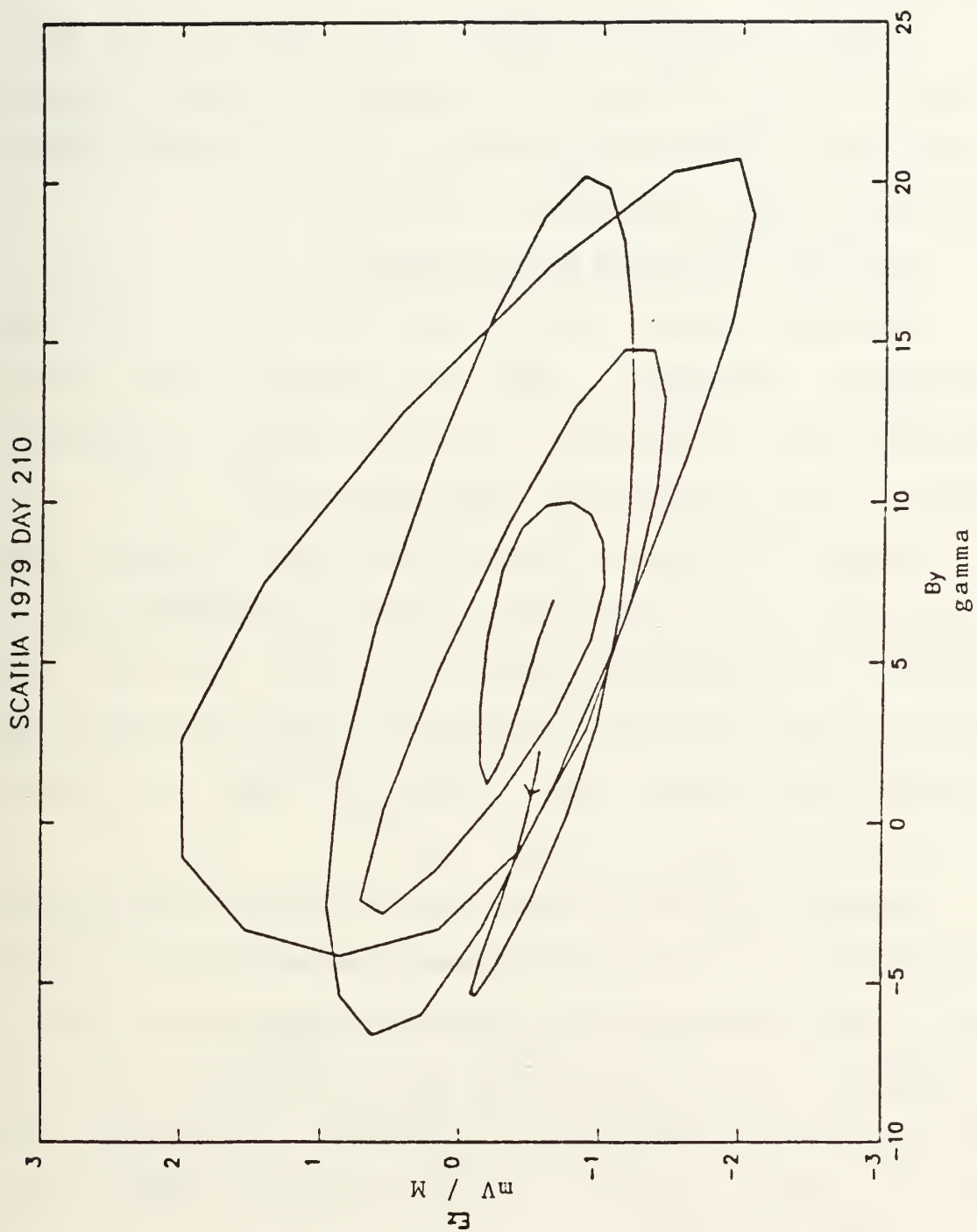
Figure 14.   Phase Plot of the Pc5 Electromagnetic Wave
(D Packet)

standing wave, where the plot becomes more circular. The average phase of $3\pi/4$ is reflected in the overall elliptical nature of the plot.

E and B are related by $E = v_\phi B$. Hence, the slope of a line, or the inclination of an ellipse, in Figure 14 gives v_ϕ. The slope of the major ellipse is 0.153 (mV/m)/(gamma) which gives a phase velocity of 153 km/sec.

2. Particle and Field Relationships

Particle count rates were measured by the UCSD electrostatic analyzers and the energy distribution functions were calculated. Ion and electron fluxes are obtained for 63 energy levels every 16 seconds.

Figure 15 contains plots of the $\log_{10} F$ versus time for low energy ions, high energy electrons, and two sets of high energy ions measured between 6.1 UT and 6.4 UT. The data sets chosen were from energy levels which exhibited the highest particle count rates. This was done in order to minimize the statistical error.

A plot of log F versus time shows the fluctuations in the energy of the ions with time. The main cause of the change in the kinetic energy of the low energy ions is the E X B force, which is generated by the Pc5 wave. In the D packet region the magnetic field strength, B_O, is approximately 140 gamma. Hence, a 2.6 mV/m electric field should give the plasma an E X B drift velocity equal to

$$v_D = \delta E_z \times B_O / |B_O^2| \sim 18.6 \text{ km/sec} \qquad (2.5)$$

40
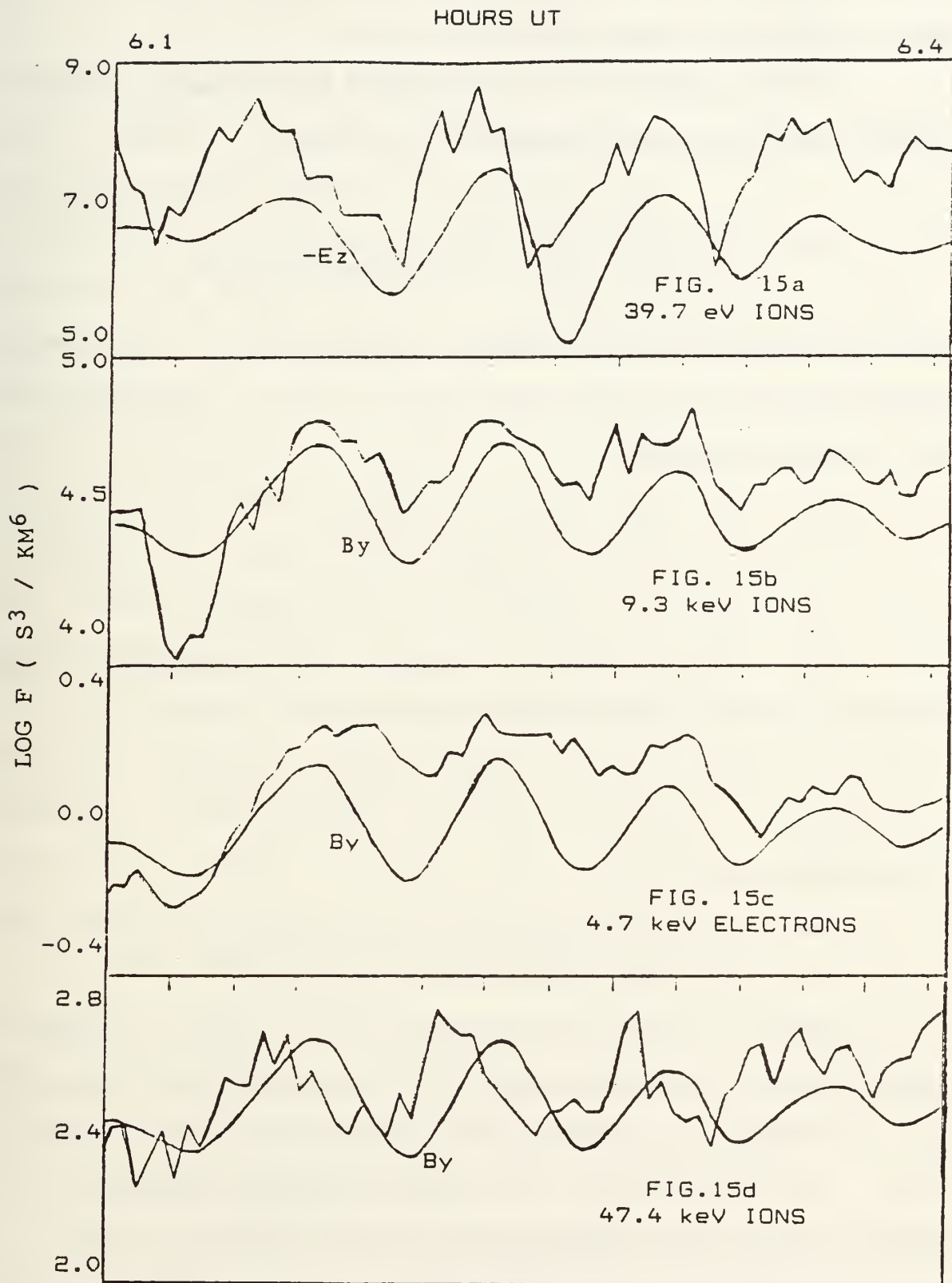
Figure 15. Ion and Electron Distribution Functions

Here the upper limit of the electric field corrected with Table 3 values is used ($\delta E \cdot \varepsilon$).

If the plasma flow is perturbed by a change in the fields, then the kinetic energy is given by

$$U = 1/2\ m\ (V - v_D)^2 \qquad (2.6)$$
$$= 1/2\ m\ (V2 - 2\ V\ v_D \cos \theta + v_D^2)$$

where V is the particle and v_D the E X B flow. If $V \gg v_D$ (which is true for 40 ev ions) and, if $\theta = 0$, then Equation (2.7) can be expanded.

$$U = 1/2\ m\ (V - v_D)^2 \qquad (2.7)$$
$$\sim 1/2\ mV^2 - (m\ V\ v_D)$$

If the particle energy distributions were Maxwellian, they could be represented by

$$F = n\ (m/2\pi kT)^{3/2}\ \exp\ -(U/kT) \qquad (2.8)$$

and by Equation (2.7)

$$\log F = \text{constant} + (\log e)\ (mV/kT) \cdot v_D$$

Hence, the plot of log F for 40 ev ions is proportional to v_D. Comparision of 39.7 ev ions with the electric field in Figure 15a shows this to be the case. The ion flux is out of phase with the electric field by π ($-E_z$ is plotted). The phase difference with the electric field is due to the unidirectional counting of the ESA's. Since they

are looking in the direction of the positive E X B force, the count rate is maximum when δE_z is negative. Thus, the low energy ion flux is modulated by the change in the flow energy induced by the E X B force. The higher energy particles respond primarily to B [Ref. 22].

Figure 15b shows that 9.3 kev ions are effectively modulated in phase with the magnetic field data. These higher energy particles are, of course, unaffected by the small change in the velocity caused by the E X B force. Hence, the changes in 9.3 kev ion flux reflect the effective motion of the different magnetic field lines with respect to the satellite. Figure 15c shows 4.7 kev electrons which, in like manner, show flux modulations in phase with the magnetic field.

At higher energies the modulation of the ion flux begins to lag the magnetic field. This is shown in Figure 15d where the flux of the 47.4 kev ions lags the magnetic field by an average of $\pi/2$. This difference reflects the large gyroradius (225 km) of these high energy particles.

These comparisons illustrate the point that the plasma is moving with the magnetic field lines of force. Hence, the plasma and the field lines oscillate together as if the particles are frozen to the field lines [Ref. 6].

3. Plasma Parameters

The plasma density, temperature and flow velocity can be determined by assuming that ion distribution

functions are nearly Maxwellian and fitting Maxwellian distributions to the data.

Analysis of the ion data requires a multi-species population due to the various masses. The distribution function becomes

$$F = \Sigma \ F_i = \Sigma \ n_i \ (m_i/2\pi kT)^{3/2} \ exp \ -(U_i/kT_i) \qquad (2.9)$$

and log F for each population is

$$log \ F = log \ \{ \ n \ (m/2\pi kT)^{3/2} \ \} - (U/kT) \ log \ e \qquad (2.10)$$
$$= f(\rho,T) - (log \ e \ / \ kT) \ U$$
$$= f(\rho,T) + f(T) \ U$$

To begin the fitting process the distribution function of the ion data is calculated and a plot of log F versus energy is made. As an example, Figure 16 shows a plot of the ion distribution function calculated from ion flux recorded by the N/S detector at 6:12 UT. This time was selected because it is near a large amplitude in the electric field. It is here that the highest drift velocities can be expected and the effect of the positive satellite potential shadowing the lowest energy ions (H^+) the smallest.

In this fitting process the plasma was assumed to contain H^+, He^+ and O^+ ions only. Once the ion species are assumed, there are three unknowns for each species in the distribution function. The temperature, kT, the density, n,

44
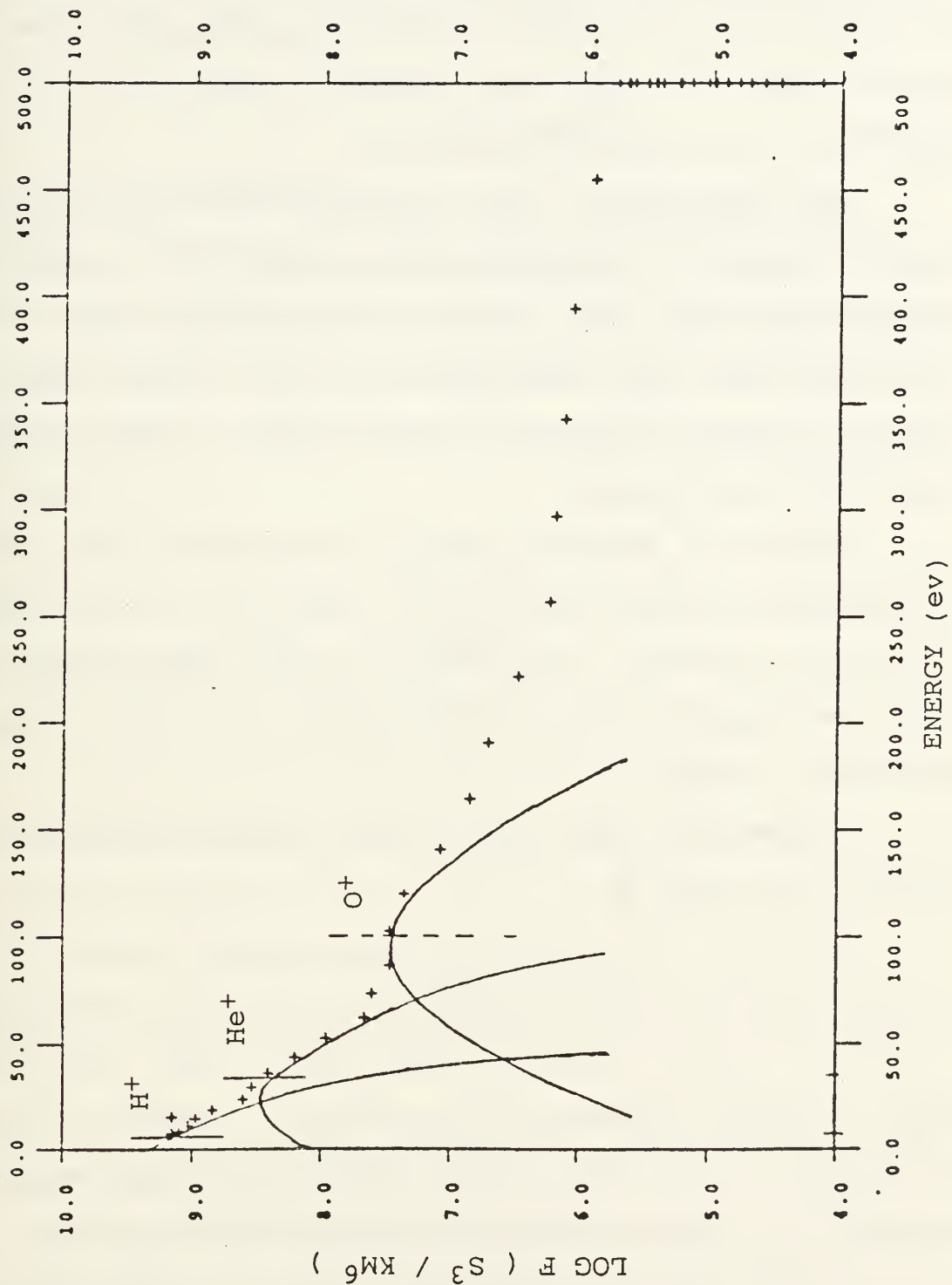
Figure 16.   UCSD Ion Distribution Function
(0 - 500) eV

45

and the flow velocity, v. A self consistent set of values is required. In particular, consistent flow velocities are required since all ions move together. One additional free parameter is the satellite potential.

The temperature, kT, is approximated to be 10 ev. In a more distinctly separated energy distribution, each ion species would show a well defined peak and the width of the peak would define the temperature. In the present case, the curvature of the distribution function is a result of both temperature and velocity.

Since the detector cannot be assumed to be looking in a direction exactly parallel to the flow, a look angle, ϕ, must be included. The choice of this angle affects the calculated density and flow velocity. In this case 10 degrees was chosen.

A peak in the distribution function determines a velocity, v_F, given by

$$v_F = (2U/m)^{1/2}$$
$$= v_D \cos \phi \qquad (2.11)$$

where v_D is the plasma drift velocity. Hence, the error introduced in the calculated velocity by an erroneous selection of the view angle is proportional to $\cos \phi$. An error of 15° in the approximation of ϕ, will cause an error in v_F of less than 10 percent. Olsen discusses this process

and shows that the error, ξ, introduced in the calculation of n is more severe [Ref. 23].

$$\xi \propto \exp -(v_D{}^2 - v_D{}^2 \cos^2\phi) \qquad (2.12)$$

In Figure 16, the peaks occur at approximately 8 ev, 35 ev and 100 ev. The lower energy peak is assumed to be due to H^+, the middle energy peak, He^+, and the highest energy peak , O^+. An approximation, v_F, for the drift velocity of each population can be made from the measured energy peak.

Since
$$V = (2U/m)^{1/2} \qquad (2.13)$$
$$v_{F\ H} \sim 39 \text{ km/s}$$
$$v_{F\ HE} \sim 41 \text{ km/s}$$
$$v_{F\ O} \sim 35 \text{ km/s}$$

In the example, Figure 16, the data are fitted with a Maxwellian distribution function for H^+, for He^+ and for O^+. Consistency requires that the Maxwellian plots for all three species have the same drift velocity and a reasonable density ratio. The values used for this fit are 35 km/s velocity, a 10 ev temperature, a look angle equal to 10 degrees, and ion number densities 1.0, 0.5, and 0.3 (cm^{-3}) for H^+, He^+ and O^+. The results of this fitting process using UCSD data over the D packet are listed in Table 4.

TABLE 4
PLASMA ION NUMBER DENSITY (1-500 ev)

Ion	n	v
	(cm^{-3})	(km/sec)
H^+	$1.27 \pm .67$	35 ± 5
He^+	$0.38 \pm .05$	35 ± 5
O^+	$0.30 \pm .10$	35 ± 5
Total	$1.95 \pm .73$	~ 35

The flow velocity of 35 km/sec contains both the flow induced by the PC5 and the steady background flow. It is estimated that the background convective flow is 1 - 10 km/sec. The steady state electric field responsible for such a flow (0.2 - 2.0 mV/m) is poorly measured by the electric field instrument. The remaining, pulsation induced flow, is approximately 25 km/sec.

From Equation (2.6), the δE_z X B_O velocity was calculated to be 18.6 km/sec. This implies a steady state flow velocity near 16.4 km/sec. Since $\delta E = v_D \cdot B_O$ and Bo = 140 gamma, a convective electric field as large as 2.3 mV/m is implied from the electric field data. Analysis throughout the D packet is consistent with this interpretation.

An alternative interpretation is that δE is twice the value measured by the floating probe. Experience with the electric field data by the principal investigator, T. L. Aggson, has suggested problems with the amplitude of the

measured fields. An aggreement within a factor of two, at this point, is considered to be supportive of the direct measurements of E.

The complete ion distribution is needed to determine the total ion density. The high energy UCSD data were combined with the high energy ion composition data from the SC8 High Energy Ion Composition Experiment [Ref. 21]. SC8 determined average ion densities in the 0.1 to 32 kev range for the one hour period from 0600 to 0700 UT. The average H^+ density was {1.974 cm^{-3}}, the He^+ density was {0.089 cm^{-3}} and the O^+ density was {0.398 cm^{-3}}. The SC8 data are shown in Figure 17. The line plot in Figure 17 is a plot of log F for the total population. The low energy (100 eV - 500 eV) O^+ ions are the same population inferred by the fitting process of the UCSD data in Figure 16. The UCSD (0 - 80 kev) ions are shown in Figure 18. The 10 keV ions are part of the bulk of the plasma sheet population, while the 47 keV ions are from the tail of the distribution function. The SC8 data are combined with the parameters obtained from the UCSD experiment and reported in Table 5.

TABLE 5
PLASMA ION DENSITIES (.01 - 32 KEV)

Ion	n
	(cm^{-3})
H^+	3.24 ± .68
He^+	0.47 ± .15
O^+	0.40 ± .17
TOTAL	4.1 ± 1.0

HIGH ENERGY IONS
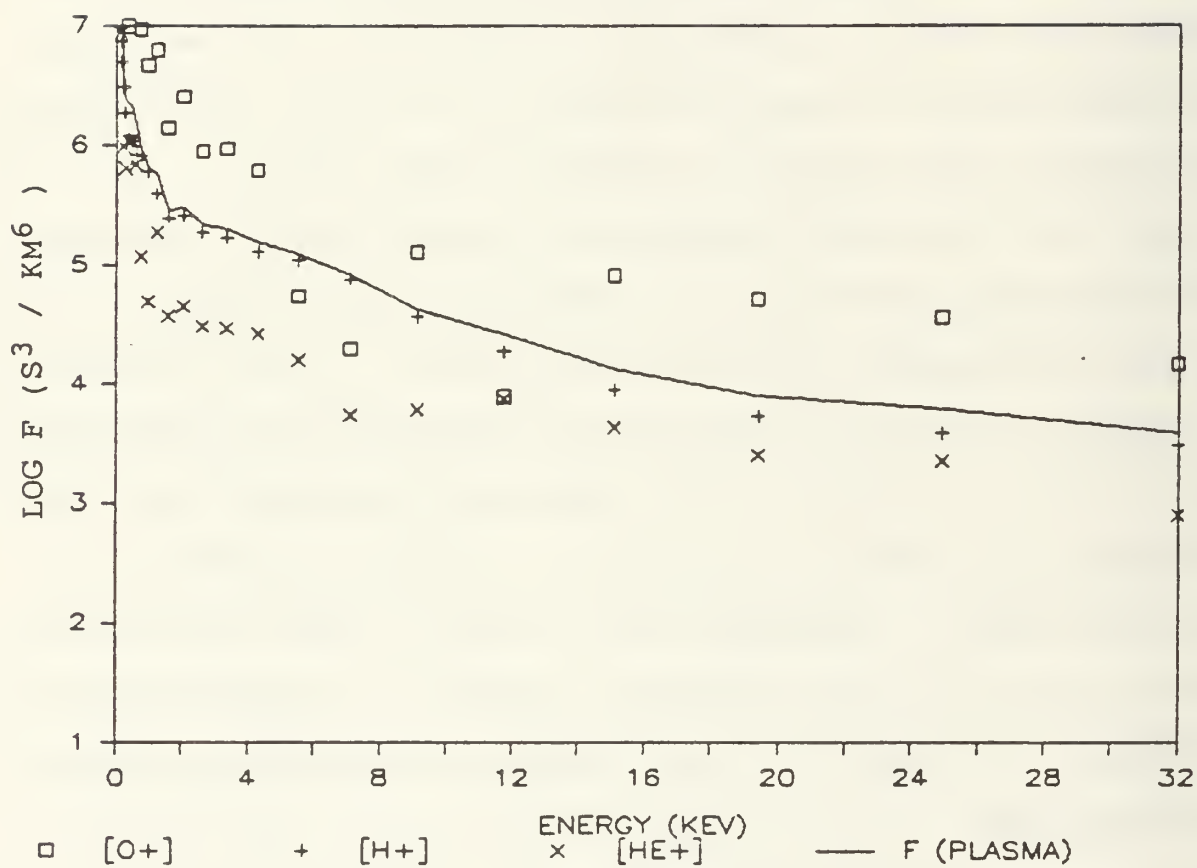
Figure 17.   SC8 Ion Distribution Function
(0.1 - 32.0) keV
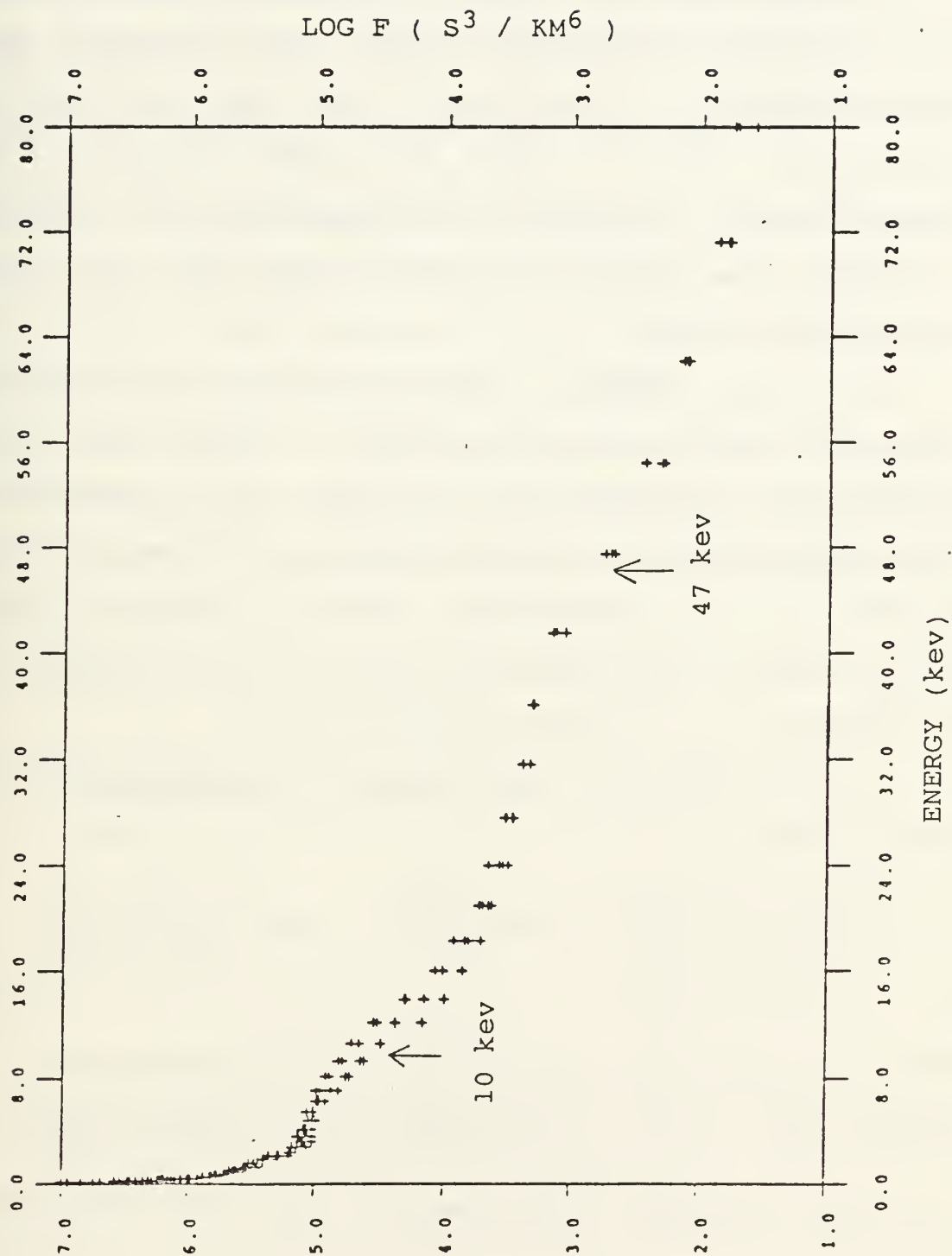
Figure 18. UCSD Ion Distribution Function

4. Electron Density

The calculation of the ion density depends largely on the distribution function of the ion population being nearly Maxwellian. An error in the look angle can introduce a large error in n. Since the number density of the electrons should be equal to the number density of the ions in a plasma, the value of n_e is a good check of the ion density calculations.

All the members of the electron population have the same mass, and that mass is known. Hence, one of the unknowns that hindered the ion calculation is removed. A useful characteristic of magnetospheric electrons is that sections of the distribution function plot have clearly defined slopes which identify different energy populations of electrons.

In a plot of the electron distribution function versus energy

$$\log F_e = \log \{n_e (m_e/2\pi kT_e)^{3/2}\} - \log e (1/kT_e) U_e$$
$$= c + b U_e \tag{2.14}$$

where b is the slope of each section of the distribution function and c is the y intercept. From Equation (2.14)

$$kT_e = -\log e / b \tag{2.15}$$

$$n_e = 10^c / (m_e / 2\pi kT_e)^{3/2}$$

52

Figure 19 is a plot of the electron distribution calculated from UCSD data taken at 6:12 UT. The units of Figure 17 are (sec^3/km^6) versus (keV). Correcting for units

$$n_e = \{10^C \times 10^{-24}\} / \{9.05 \times 10^{-13} / kT \, (ev) \}^{3/2} \tag{2.16}$$

In Figure 19 two energy sets of electrons are identified. By the slope intercept method, the 17.5 kev electrons are shown to have a number density of 0.007 cm^{-3}. The number density of the 1.65 kev electrons is shown to be 1.77 cm^{-3}. By expanding the lower energy section of this data two other electron groups were identified. The number densities which were calculated for each set of electrons is reported in Table 6.

TABLE 6
ELECTRON NUMBER DENSITY

Energy Range (kev)	Temperature (kev)	n (cm^{-3})
15 - 80	17.50	0.007 ± .001
1.0 - 15	1.65	1.77 ± .09
0.2 - 1.0	0.71	1.46 ± .09
0.0 - 0.2	0.12	0.67 ± .04
TOTAL		3.9 ± .2

Hence, the calculated ion number density (4.1 cm^{-3}) is consistent with the independently determined electron density.
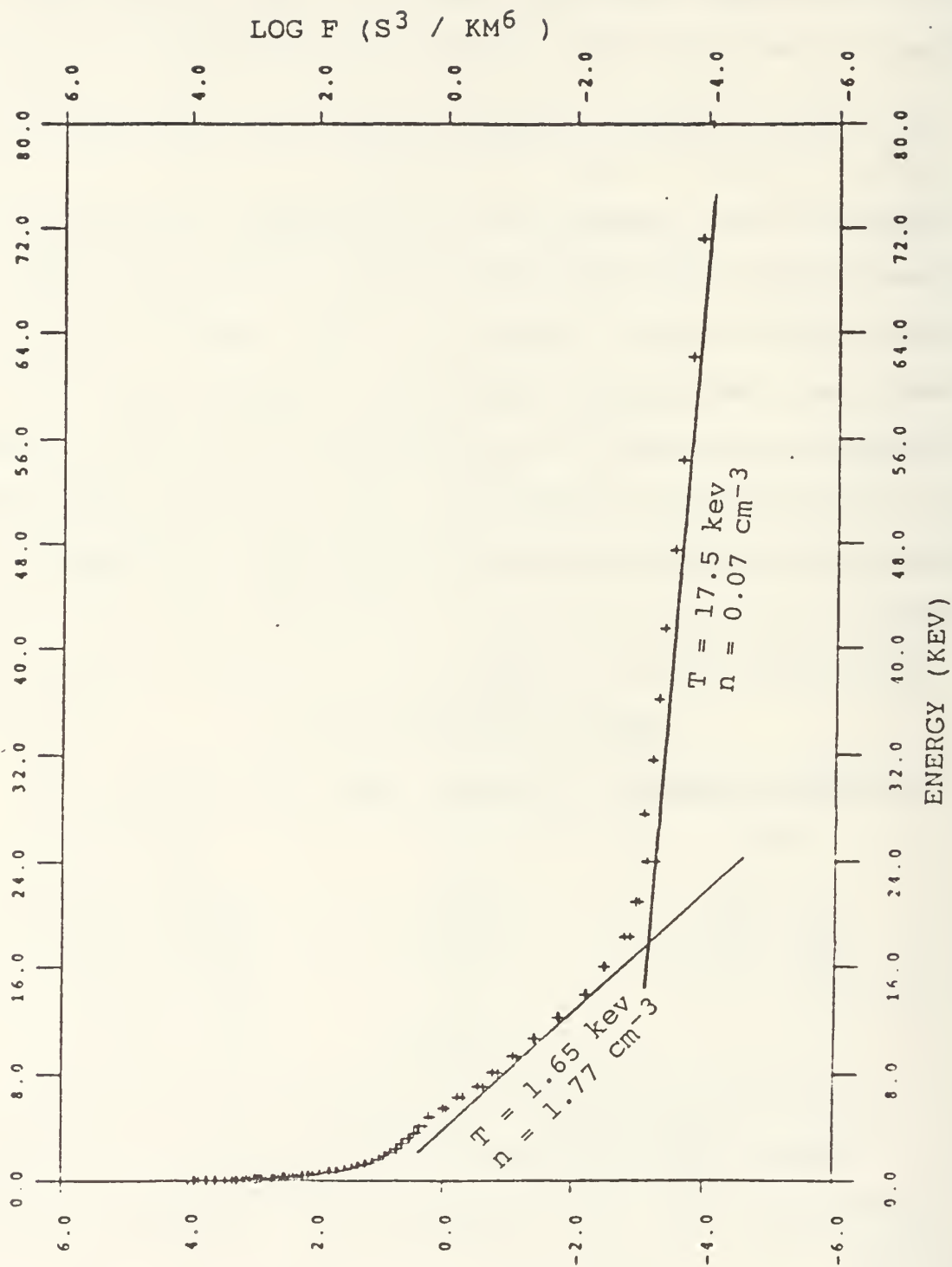
Figure 19.   UCSD Electron Distribution Function
(0 - 80) keV

54

5. Self Consistency of the Data

It is now important to determine whether these numbers represent a self-consistent relationship between n, B, E and v. Since the plasma acts as a parallel resistive circuit on the electric field antenna, a major concern is to verify the amplitude measurements of E_z.

Cummings used the following equation to deduce the density of the ambient plasma from field and particle data measured by the ATS-6 spacecraft in geosynchronous orbit

$$n = \delta B^2 / \mu_o \langle m \rangle v_D^2 \tag{2.17}$$

where $\langle m \rangle$ is the average particle mass [Ref. 7]. This relationship is used to investigate the consistency of the ion density calculations.

Assuming that the plasma is made up of H^+, He^+ and O^+, and using the values from Table 6, the ion mass density is given by

$$\rho = \Sigma\, n_i\, m_i \tag{2.18}$$
$$= \{3.24(1) + .47(4) + .40(16)\}\, m_p$$
$$\rho = (11.52\, m_p)\, kg/cm^3$$

and
$$\langle m \rangle = \rho / n = 2.81\, m_p$$

where
$$m_p = 1.672 \times 10^{-27}\, kg.$$

Equation (2.17) is then rewritten,

$$v^2 = \delta B^2 / \mu_0 \langle m \rangle n$$

$$v = \delta B / (\mu_0 \rho)^{1/2}$$

Since
$$|v| = |\delta E / B_0|$$

$$\delta E = \delta B \, B_0 / (\mu_0 \rho)^{1/2} \tag{2.19}$$

$$= 6.4 \times 10^{-3} \, (\delta B \, B_0) \quad mV/m$$

where the units of δB and B_0 are gamma.

In the D packet
$$B_0 = 140 \text{ gamma}$$

$$6 < \delta B_y < 12 \text{ gamma} \tag{2.20}$$

Therefore the magnitude of the electic field inferred by mass density is

$$5.4 < \delta E < 10.8 \quad mV/m \tag{2.21}$$

The measured values of δE_z were

$$0.62 \leq \delta E_z \leq 1.8 \; mV/m \tag{2.22}$$

Taking into account the electric field correction factor of 1.43, from Table 4, the magnitude of the perturbed electric field is calculated to be

$$0.9 < \delta E_p < 2.6 \; mV/m \tag{2.23}$$

These values are a factor of 3 lower than predicted by Equation (2.21). A factor of 2 could be accounted for if

the impedance of the plasma was comparable to the internal impedance of the electric field experiment (this is roughly the case). A small error, not larger than a factor of 2, in the electric field data is implied by the comparison.

6. The Alfven Velocity

The same comparison can be made in terms of velocities. The Alfven velocity is

$$V_A = \omega/k = B_o / (\mu_o \rho)^{1/2} \tag{1.2}$$

Since $\qquad$ Curl E = -dB/dt

then $\qquad$ $ik\ E_p \sim -(-i\omega)\ B_y$

and $\qquad$ $\delta E_p/B_y \sim \omega/k = V_A \tag{2.24}$

Using upper and lower bounds of the field amplitudes given by Equations (2.20) and (2.23), the Alfven velocity calculated from measured E is

$$328\ km/sec < V_A < 378\ km/sec \tag{2.25}$$

Using the ion density relationship

$$V_A = B_o / (\mu_o \rho)^{1/2} = 900\ km/sec \tag{2.26}$$

The electric field data appears to be low by a factor of 3 in this comparison.

7. The Poynting Vector

The nature of the propagation of the PC5 can be seen by examining the relationship of δE_z and δB_y. If the

micropulsation was a classical plane Alfven wave, then

$$\vec{S} = (1/\mu) \; \vec{E} \times \vec{B}$$

$$\sim (1/\mu_o) \; \delta\vec{E} \times \delta\vec{B}$$

$$\sim \hat{i} \; (1/\mu_o) \; (\delta E_y \; \delta B_z - \delta E_z \; \delta B_y)$$

which assumes the other components of the Poynting vector are small. δE_y is not measured, but δB_z is small, so

$$\vec{S} \sim \hat{i} \; (1/\mu_o) \; (-\delta E_z \; \delta B_y) \qquad (2.27)$$

In Figure 20 Px = $(\delta E_z \; \delta B_y)$, so

$$\vec{S} = -\hat{i} \; (1/\mu_o) \; (Px) \times 10^{-12} \; \text{Watts/m}^2 \qquad (2.28)$$

The negative values of Px in Figure 20 indicate that the wave is propagating in the +X direction, northward along the magnetic field line. The wave must have been generated south of 7° N. The fact that Px is, at times, zero or positive indicates that the micropulsation is not a simple traveling wave, but is superimposed on a smaller wave traveling in the southward direction. This is the mixed standing / propagating nature inferred previously in Figure 14.

And finally, the magnitude of the Poynting vector is calculated

$$Px = (1.8 \quad mV/m) \; (-12 \; gamma)$$

$$|S| = (1/\mu_o) \; |Px| \times 10^{-12} \qquad (2.29)$$

$$= 17.2 \; \mu\text{Watts/m}^2$$

58
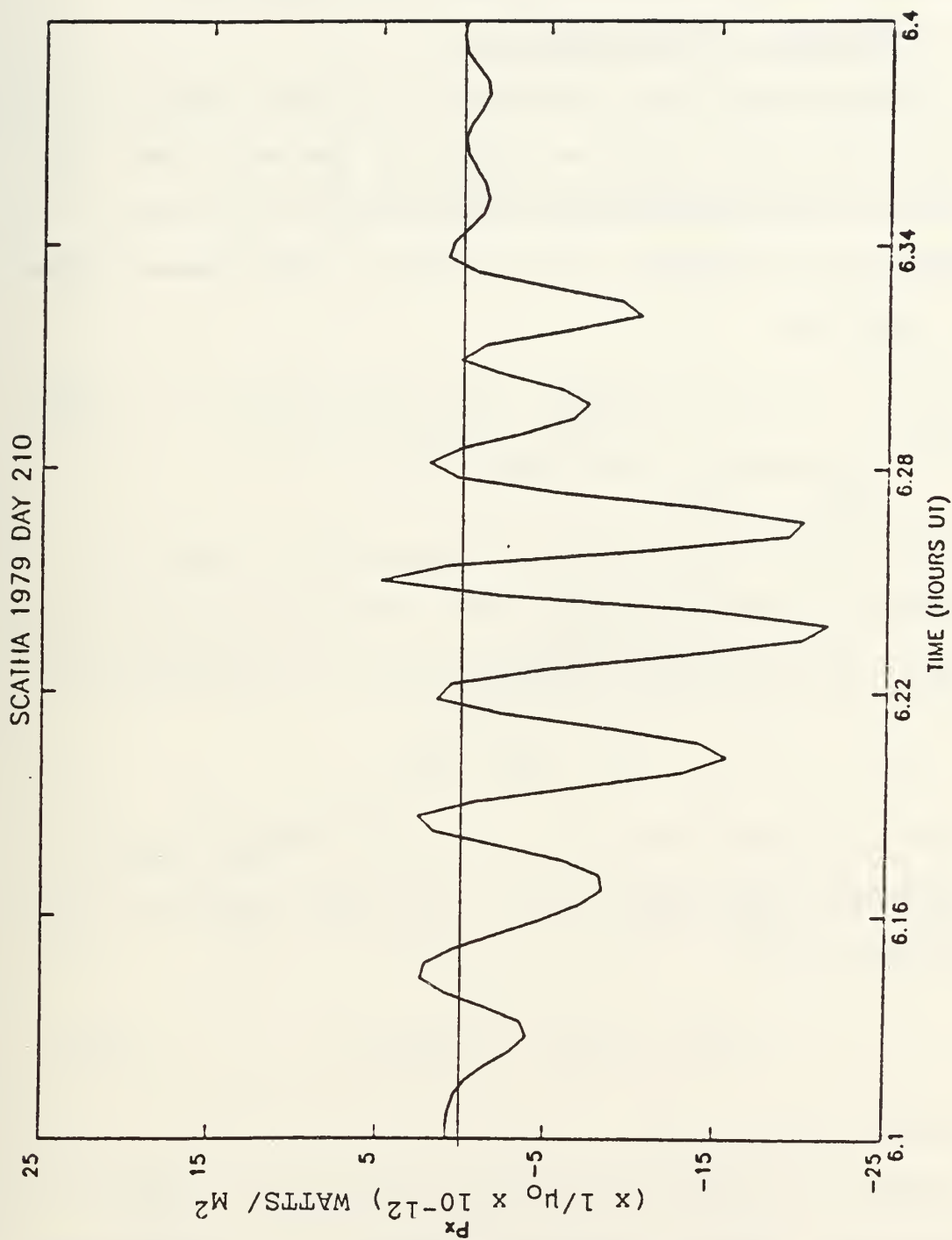
Figure 20.   The Poynting Vector
(Calculated in the D Packet)

This presumes that the electric field measurement is correct. Given the possible error in δE, the magnitude of the Poynting vector could be as high as 50 μWatts/m^2.

8. Dependence of the Period on L

The period of the Pc5 depends on the length of the field line and the Alfven velocity of the wave [Ref. 24]. The variation of micropulsation period with latitude can be expressed as a function of L and n, the plasma number density. [Ref.25].

$$\tau = (2\pi\ L^4\ R_E/B_E) \cdot (\mu_O\ \langle m \rangle\ n/\Omega)^{1/2} \qquad (2.30)$$
$$B_E = 3.12 \times 10^{-5} \text{ Tesla}$$

Ω is proportional to an Alfven wave eigenvalue which is calculated for different values of L, density gradient, and wave type. In a simpler form this equation corresponds to

$$\tau = 2\pi\ (m/k)^{1/2} .$$

The SCATHA data can be used to determine the dependence of the period of this Pc5 on L. If the period, τ, is proportional to L^m

$$\log \tau = \log C + m \log L \qquad (2.31)$$

where C is a constant.

Figure 21 shows the average micropulsation period in each resonance packet, plotted against L. The slope, determined by linear regression, is 3.96 $\pm$ .07. Hence, the
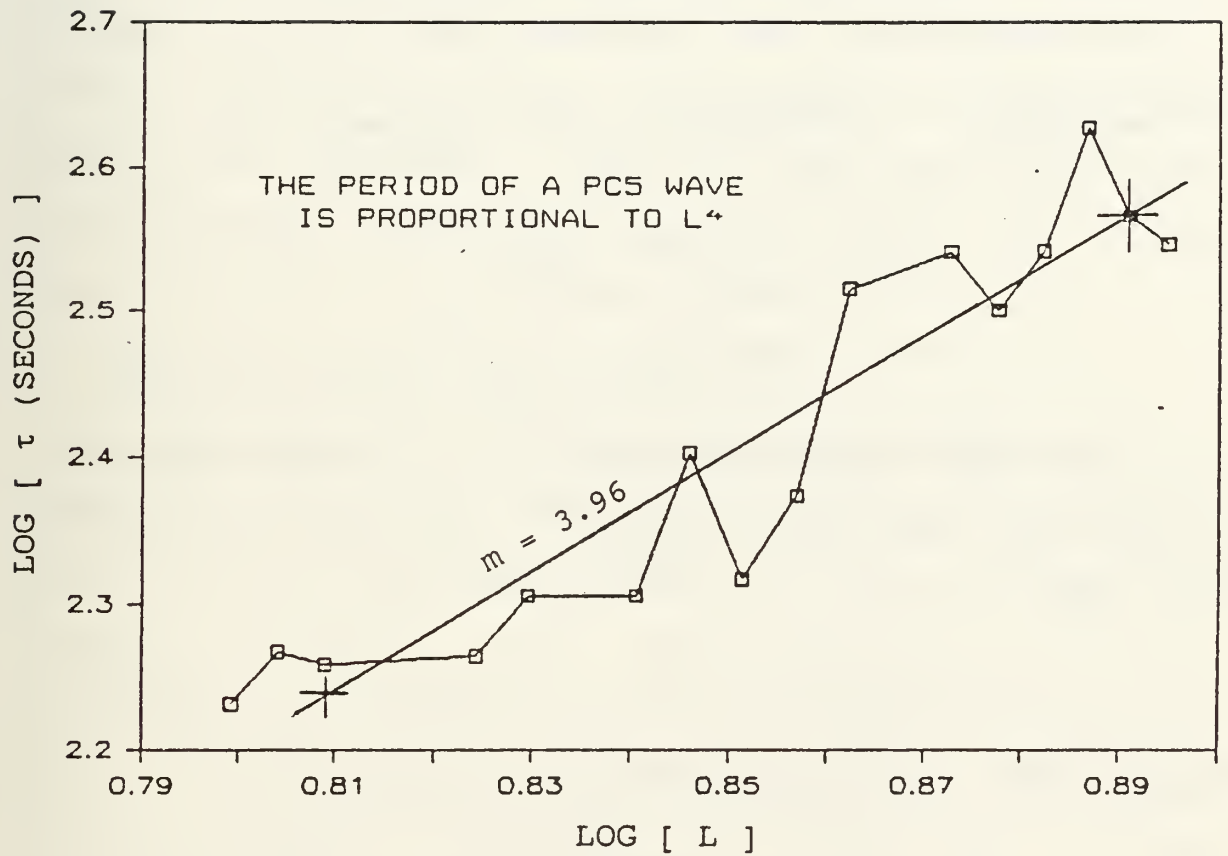
Figure 21. Pc5 Period Versus McIlwain L

SCATHA data is in close agreement with the theoretical relationship

$$\tau \propto L^4 \qquad (2.32)$$

Having verified the L dependence of the period, Equation (2.30) is rewritten and utilized to predict a mass density to compare with the previous measurements.

$$\rho = n \langle m \rangle = (\tau \, B_E \, / \, 2\pi \, L^4 \, R_E \,)^2 \, x \, (\Omega \, / \, \mu_o) \qquad (2.33)$$

For the values τ = 224 sec (in the D packet)

$$L = 7.0$$

$$B_E = 3.12 \times 10^{-5} \text{ Tesla}$$

$$n \langle m \rangle = 2.514 \, m_p \cdot \Omega \quad (cm^{-3}) \qquad (2.34)$$

Orr and Matthew calculate Ω for a toroidal mode wave in plasma density gradients which obey power laws between R^4 and R^2 [Ref. 25]. At L = 7 these values are

$$3.6 \text{ (for } R^4) < \Omega < 4.2 \text{ (for } R^2) \qquad (2.35)$$

The mass density inferred by Equation (2.33) is

$$\underline{9.05 \, m_p < n \langle m \rangle < 10.56 \, m_p \quad (cm^{-3})} \qquad (2.36)$$

The measured mass density was 11.52 m_p (cm^{-3}). If the theoretical relationship is valid for this Pc5 (it has been shown that it is substantively valid by the agreement with the power law of the period), then the difference between

62

predicted particle density and measured density implies that the mass density has been slightly overestimated. However, a deviation of the wave period of only 10 seconds from the average period, used in Equation (2.34), would bring the predicted mass density into exact agreement with the measured mass density.

Since the values for Ω were derived from a theoretical eigenvalue equation for the toroidal wave, complete aggreement with the mass density results of this study is not demanded. However, this comparison shows strong agreement with both variables, L and ρ. The plasma density gradient is the unknown variable.

C. SOLAR AND MAGNETIC FIELD CONDITIONS

Geomagnetic and Solar Data, published by the Journal of Geophysical Research, indicates that Day 210 was a moderately active day, Kp = 3 to 5, with no magnetic substorms recorded. Forty eight hours prior to the Pc5 event there was a period of very high magnetic activity in which a 12 hour magnetic storm occurred [Ref. 26]. These conditions support the statement by Jacobs [Ref. 1] that Pc5's generally occur during recovery periods following magnetic disturbances.

D. OTHER OBSERVERS

SCATHA observed the Pc5 at 331 degrees east longitude on L = 7. Magnetograms from the National Institute of Polar

Research from the conjugate ground stations at Leirvogur, Iceland (68.2° N 338.3° E) and at Syowa Base, Antarctica (69.0° S 39.6° E) indicate that this event was observed at these stations simultaneously from 0600 to 0700 UT. The time resolution of the ground station data was not clear enough to say more. These stations are located at the invariant latitude for L = 7. The simultaneous observation of this event would imply that the generation was occuring near the equator.

There is no indication of this observation at Narssarssuaq Station, Greenland (61.2° N 314.2° E) or at St. Johns Station (47.6° N 307.3° E). Magnetograms from the NOAA GOES 2 and GOES 3 satellites were also scanned. They showed frequent magnetic activity, but none which could be correlated with the Pc5. These satellites were in geosynchronous orbit at 252° East and 225° East respectively.

The lack of Pc5 activity at locations west of the SCATHA sector indicates a limit on the temporal and spatial extent of the event. The Pc5 appears to have been confined to 45 degrees of longitude in the morning sector observed by SCATHA.

III. DISCUSSION

A. THE CHARACTER OF THE PC5

In Chapter II, the observable quantities characterizing this Pc5 event were investigated by focusing on data taken at the temporal and spatial center of the event. The wave was shown to be   a   traveling Alfven   wave   guided by the magnetic field line.   The Alfven velocity was nearly 900 kilometers per second. A calculation of the Poynting vector showed the wave was traveling northward.

The electromagnetic field perturbation was shown to be occuring in a plane perpendicular the the magnetic field line. The magnetic field lagged the electric field by $3\pi/4$. The amplitude of the magnetic field perturbations was near 12   gamma.   The   measured   electric   field   reached 2.57 millivolts per meter. By requiring consistency of the data, the measured electric field was shown to be low by a factor of 2 to 3. The period of the Pc5, at L=7, was 224 seconds and the period of the wave was shown to be proportional to L^4.

The plasma density was estimated to be 1.9 x 10^{-23} (gm/cm^3).   The ion number density was determined to be 4.1 (cm^{-3}). This is consistent with previous magnetospheric studies.   The   calculation of the Alfven velocity ~ 900 km/sec is also consistent with previous studies.   Most

recently, empirical models of average magnetospheric plasma and field data were developed to study Alfven and Fast Mode wave speeds [Ref. 27]. These models predict plasma densities of 3-5 (cm^{-3}), plasma temperatures of 30-100 ev and Alfven wave speeds of 500 - 1000 km/sec at L = 7.0 in the morning sector of the magnetosphere.

B. SPATIAL EXTENT OF THE PC5

The most interesting factor in this Pc5 event is the packetized nature of the micropulsation resonances through this sector of the magnetosphere. The breadth and location in these regions is presented in Table 7.

TABLE 7
RESONANCE PACKET LOCATION AND SIZE

t (UT)	ID	Width (km)	Latitude (° N)	L	Local Time	Γ
4.66	A	5300	7.38	7.8	2:45	0.45
5.25	B	5300	7.50	7.5	3:23	0.50
5.84	C	4200	7.45	7.2	3:54	0.32
6.26	D	3300	7.29	6.9	4:21	1.00
6.80	E	3600	6.96	6.7	4:55	0.72
7.46	F	5400	6.11	6.4	5:42	0.49

The Γ factor, in Table 7, is a normalized resonance strength for each region, which is the ratio of the electric field amplitude in a region to the electric field in the D packet. These resonance regions are seperated by sectors of low resonance which vary in distance from 1200 kilometers to 3600 kilometers.

C. UNRESOLVED ISSUES

A complete understanding of this event would require a vector description of the data. There are significant aspects of the Pc5 which were neglected by this study. One is the effect that the nutation of the spacecraft spin axis has on the raw data. The nutation effect can be seen as a small pulsation in each component of the magnetic field data in Figure 8. Another aspect is the significance of the smaller component of the Pc5 which is in the radial direction, B_z. The B_z component has an average amplitude of 4 gamma. This component has a small effect on the amplitude of the Pc5 magnetic field, but has a significant effect on the rotational motion of the field. A study that included this component would provide a more realistic description of the Pc5 event.

A most difficult aspect, which is left for the student who follows this study, is the separation of the spatial character of the event from the temporal description which this study provides. Many of the effects seen in the data, such as the sinusoidal variation of the resonance in each packet, have been described but not explained.

D. RECOMMENDATIONS

1. The spatial and temporal extent of this Pc5 could not be determined by SCATHA alone. Specifically, it is not known if local dawn was a boundary of the Pc5 or that the Pc5 ended at all locations at 6:56 UT. The radial boundaries

of the event are also left unresolved. The observation of the Pc5 ended when SCATHA passed L = 6.6. This may have been a coincidence, but it could be a major characteristic of this phenomenon. A correlation with a satellite that was East of SCATHA could provide an answer (such data may be available from the European GEOS-2 satellite). Better time resolution of the conjugate ground station data would determine the location of the generating mechanism.

2. Approximate densities were calculated in the region of highest resonance, the D packet. The wealth of information made available by SCATHA provides an area for further study into the magnetospheric plasma profile between 5.5 and 7.5 Re.

3. The theoretical models presently available describe standing and compressional Alfven waves. Since this event provides extensive data from a traveling wave event, further investigation into this area of micropulsation theory is warranted.

4. Theorists have recently shown great interest in understanding the resonance conditions for Alfven waves. As emphasized in this paper, the packetized nature of the resonance conditions in the morning sector of the magneto-sphere is displayed vividly by the SCATHA data. These observations should be used to improve the understanding of Alfven wave resonance.

IV. CONCLUSIONS

Observations of a Pc5 event occuring between L = 6.6 and L = 8.0 in the pre-dawn sector of July 29, 1979, at 7° N, were reported. Hydromagnetic resonance regions spanning 3000 to 5000 kilometers with centers separated by 2400 kilometers were identified.

The plasma density in the highest resonance region was shown to be 1.92×10^{-23} gm/cm^3. Ion flux at 40 ev was shown to be in phase with the electric field . Ion fluxes at 9 kev, and 5 kev electrons, were shown to be in phase with the magnetic field. The 47 kev ions lagged the magnetic field by $\pi/2$ radians.

Particle data from the UCSD electrostatic analyzers was shown to be an effective means of cross checking electric field data. The electric field data was assumed to be a projection of the perturbation electric field onto SCATHA's antenna. By comparing this data with ion density predictions, the amplitude of the measured electric field data was shown to be a factor of 2 - 3 too low to be consistent with the complete set of data (this is considered to be a small error).

The periods of the micropulsations, between L = 6.3 and 7.7, were shown to be proportional to the fourth power of L, which supports present models of resonant Alfven wave

activity in the magnetosphere. Alfven velocities were shown to be nearly 900 kilometers per second within high resonance regions of the event.

The electromagnetic pulsations were in a plane perpendicular to the magnetic field line. In the Pc5, the magnetic field lagged the electric field by $3\pi/4$. The Poynting vector was shown to be in the direction of the main magnetic field vector, confirming that the wave was a traveling Alfven wave. Simultaneous observations by conjugate ground stations indicated that the generation could be occurring at the equator.

The unique packetized resonance regions exhibited by this PC5 as well as the non-classical wave character of this event indicates that further theoretical study utilizing data from SCATHA is warranted.

LIST OF REFERENCES

1. Jacobs, J. A., Geomagnetic Micropulsations, Springer-Verlag Berlin, 1970.

2. Stewart, B., "On the Great Magnetic Distrubance which which extended from August 27 to September 7, 1858," Transcripts of the Royal Society of London, v. 423, 1861.

3. Barfield, J. N. and R. L. McPherron, "Statistical Characteristics of Storm Associated Pc5 Micropulsations Observed at the Synchronous Equatorial Orbit," Journal of Geophysical Research, v. 77, pp. 4720-4733, 1972.

4. Barfield, J. N., R. L. McPherron, P. J. Coleman, Jr. and D. J. Southwood,"Storm-Associated Pc5 Micropulsation Observed at the Synchronous Equatorial Orbit," Journal of Geophysical Research, v. 77, pp. 143-158, 1972.

5. Lanzerotti, L. J., H. Fukunishi, C. C. Lin and L. J. Cahill, "Storm Time Pc5 Magnetic Pulsation at the Equator in the Magnetosphere and Its Latitude Dependence as Measured on the Ground," Journal of Geophysical Research, v. 29, p. 2420, 1974.

6. Chen, Francis F., Introduction to Plasma Physics and Controlled Fusion, 2nd ed. v. 1, pp.136-140, Plenum Press, 1984.

7. Cummings, W. D., S. E. Deforest and R. L. McPherron, "Measurements of the Poynting Vector of Standing Hydromagnetic Waves at Geosynchronous Orbit," Journal of Geophysical Research, v. 83, pp. 697-706, 1978.

8. Waite, J. H., D. Gallagher, M. Changler, R. Olsen, R. Comfort, J. Johnson, C. Chappell, W. Peterson, D. Weimer and S. Shawhan, "Plasma and Field Observations of a Pc 5 Wave Event," Journal of Geophysical Research, v. 91, pp.11147-11161, 1986.

9. Matthews, John, "Hydromagnetic Wave Activity Detected by the GEOS 2 Double-Probe Experiment During 1979," Journal of Geophysical Research, v. 92, pp. 7423-7431, 1987.

10. Takahashi, K., J. F. Fennell, E. Amata and P. R. Higbie, "Field Aligned Structure of the Storm Time Pc5 Wave of November 14-15, 1979," Journal of Geophysical Research, v. 92, pp. 5857-5864, 1987.

11. Alfven, H., "On the Existence of Electromagnetic-Hydromagnetic Waves," Arkiv for Matematik, v. 29B No. 2, 1943.

12. Lundquist, S., "Studies in Magneto-Hydrodynamics," Arkiv for Fsyik, v. 5, pp. 297-347, 1952.

13. Alfven, H., Cosmical Electrodynamics, Oxford University Press, 1950.

14. Sugiura, M. and C. R. Wilson, "Oscillation of the Geomagnetic Field Lines and Associated Magnetic Perturbations at Conjugate Points," Journal of Geophysical Research, v. 69, pp. 1211-1216, 1964.

15. Hasegawa, A., and L. Chen, "Theory of Magnetic Pulsations," Space Science Reviews, v. 16, pp. 347-359, 1974.

16. Olsen, R. C., T. Aggson and B. Ledley, "Observations of Electric Fields Near Plasmapause at Midnight," Journal of Geophysical Research, v. 91, pp. 12017-12019, 1986.

17. Craven, P. D., R. Olsen, J. Fennell, D. Croley and T. Aggson, "Potential Modulation of the SCATHA Spacecraft," Journal of Spacecraft, v. 24, pp. 150-151, 1987.

18. McIlwain, Carl E., "Magnetic Coordinates," Space Science Reviews, v. 5, pp. 585-598, 1966.

19. Hess, Wilmot H., Introduction to Space Science, pp. 41-58, Gordon and Bresch Science Publishers, Inc., 1965.

20. Fennell, J. F., "Description of the P78-2 (SCATHA) Satellite and Experiments," The IMS Source Book, American Geophysical Union, pp. 65-81, 1982.

21. Air Force Systems Command SAMSO TR-78-24, Description of the Space Test Program and Payloads, pp. 29-56, October 31, 1978.

22. Southwood, David J. and Margaret G. Kivelson, "Charged Particle Behavior in Low-Frequency Geomagnetic Pulsations; 1. Transverse Waves," Journal of Geophysical Research, v. 86, pp. 5643-5655, 1981.

23. Olsen, Richard Christopher, "Field-Aligned Ion Streams in the Earth's Midnight Region," <u>Journal of Geophysical Research</u>, v. 87, pp. 2301-2310, 1982.

24. Singer, H. J., D. J. Southwood, R. J. Walker and M. G. Kivelson, "Alfven Wave Resonances in a Realistic Magnetospheric Field Geometry," <u>Journal of Geophysical Research</u>, v. 86, p. 4593, 1981.

25. Orr, David and James A. D. Matthew, "The Variation of Geomagnetic Micropulsation Periods with Latitude and the Plasmapause," <u>Planetary and Space Science</u>, v. 19, p. 899, 1971.

26. Lincoln, J. Virginia,"Geomagnetic and Solar Data," <u>Journal of Geophysical Research</u>, v. 84, No. A11, 1979.

27. Moore, T. E., and others,"MHD Wave Breaking in the Outer Plasmasphere," <u>Geophysical Research Letters</u>, v. 14, pp. 1007-1010, 1987.

INITIAL DISTRIBUTION LIST

No. Copies

1. Defense Technical Information Center   2
   Cameron Station
   Alexandria, Virginia 22304-6145

2. Library, Code 0142   2
   Naval Postgraduate School
   Monterey, California 93943-5002

3. Dr. K. Woehler, Chairman   2
   Physics Department
   Naval Postgraduate School
   Monterey, California 93943-5002

4. Dr. R. C. Olsen   20
   Physics Department, 61-Os
   Naval Postgraduate School
   Monterey, California 93943-5002

5. Mr. R. Gracen Joiner   1
   Office of Naval Research
   Code 1114SP
   800 North Quincy Street
   Arlington, Virginia 22217

6. Henry R. Radoski   1
   Air Force Office of Scientific Research
   Bolling Air Force Base
   AFOSR/NP Bldg #410
   Washington, D.C. 20332

7. Dr. Margaret Kivelson   1
   Institute of Geophysics and Planetary Physics
   University of California at Los Angeles
   Los Angeles, California 90024

8. Dr. Robert McPherron   1
   Institute of Geophysics and Planetary Physics
   University of California at Los Angeles
   Los Angeles, California 90024

9. Dr. Paul Higbie   1
   Mail Stop D438
   Los Alamos National Laboratory
   Los Alamos, New Mexico 87545

10. Dr. T. L. Aggson   1
    MC 696
    NASA/GSFC
    Greenbelt, Maryland   20771

11. Dr. B. Ledley   1
    MC 696
    NASA/GSFC
    Greenbelt, Maryland 20771

12. Dr. Jack Quinn   1
    Department 91-20/Bldg 255
    3251 Hanover Street
    Palo Alto, California   94304

13. Dr. C. E. McIlwain   1
    C-011
    Center for Astrophysics and Space Science
    University of California at San Diego
    La Jolla, California   92093

14. Dr. Liu Chen   1
    Princeton Plasma Physics Labs
    P.O. Box 451
    Princeton, New Jersey   08544

15. Dr. Akira Hasegawa   1
    Tohoku University
    Obs Center Earth Pr
    Sendai, Japan 980

16. Dr. Arne Pedersen   1
    Space Science Department
    ESA/ESTEC
    P.O. Box 299
    2200 AG Noordwijk
    The Netherlands

17. Dr. R. Schmidt   1
    Space Science Department
    ESA/ESTEC
    P.O. Box 299
    2200 AG Noordwijk
    The Netherlands

18. Dr. Kazue Takahashi   1
    Johns Hopkins University
    Applied Physics Laboratory
    Johns Hopkins Road
    Laurel, Maryland   20707

19. Dr. T. Potemra   1
    Johns Hopkins University
    Applied Physics Laboratory
    Johns Hopkins Road
    Laurel, Maryland 20707

20. Dr. Mark Engbretson   1
    Augsburg College
    731 21st Avenue South
    Minneapolis, Minnesota 55454

21. Dr. Hunter Waite   1
    Mail Code E253
    NASA/MSFC
    Huntsville, Alabama 35812

22. Dr. T. Moore   1
    Mail Code E253
    NASA/MSFC
    Huntsville, Alabama 35812

23. Dr. M. Chandler   1
    Mail Code E253
    NASA/MSFC
    Huntsville, Alabama 35812

24. Dr. J. Horwitz   1
    Physics Department
    The University of Alabama in Huntsville
    Huntsville, Alabama 35899

25. Dr. R. H. Comfort   1
    Physics Department
    The University of Alabama in Huntsville
    Huntsville, Alabama 35899

26. Dr. J. Fennell   1
    M2/259
    Aerospace Corporation
    P.O. Box 92957
    Los Angeles, California 90009

27. Dr. David Southwood   1
    Department of Physics
    Prince Consort Road
    Imperial College of Science and Technology
    London, England SW7

28. Dr. Brian Fraser   1
    Department of Physics
    Newcastle University
    Newcastle, NSW
    Australia 2308

29. Dr. Tsugunobu Nagai   1
    Meteorological Research Institute
    1-1 Nagamine
    Yatabe, Ibariki
    305 Japan

30. Dr. David Orr   1
    Department of Physics
    University of York
    York, England Y01 5DD

31. Lt. John W. Patterson   1
    Stu SWOSCOLCOM
    NETC
    Newport, Rhode Island 02841